Atmos. Chem. Phys. Discuss., 9, 17705–17751, 2009
www.atmos-chem-phys-discuss.net/9/17705/2009/

Atmospheric Chemistry and Physics Discussions

This discussion paper is/has been under review for the journal *Atmospheric Chemistry and Physics (ACP)*. Please refer to the corresponding final paper in *ACP* if available.

Fluorescent biological aerosol particle concentrations and size distributions measured with an ultraviolet aerodynamic particle sizer (UV-APS) in Central Europe

J. A. Huffman[1], **B. Treutlein**[1,*], **and U. Pöschl**[1]

[1]Max Planck Institute for Chemistry, Biogeochemistry Department, Becherweg 27, 55128 Mainz, Germany
[*]now at: Ludwig Maximilians University, Institute for Physical Chemistry, Munich, Germany

Received: 24 July 2009 – Accepted: 13 August 2009 – Published: 28 August 2009

Correspondence to: U. Pöschl (poeschl@mpch-mainz.mpg.de)

Published by Copernicus Publications on behalf of the European Geosciences Union.

Abstract

Primary biological aerosol particles (PBAPs), including bacteria, spores and pollen, are essential for the spread of organisms and disease in the biosphere, and numerous studies have suggested that they may be important for atmospheric processes, including the formation of clouds and precipitation. The atmospheric abundance and size distribution of PBAPs, however, are largely unknown. At a semi-urban site in Mainz, Germany, we used an ultraviolet aerodynamic particle sizer (UV-APS) to measure fluorescent biological aerosol particles (FBAPs), which can be regarded as viable bioaerosol particles representing a lower limit for the actual abundance of PBAPs. Fluorescence of non-biological aerosol components are likely to influence the measurement results obtained for fine particles (<1 µm), but not for coarse particles (1–20 µm).

Averaged over the four-month measurement period (August–December 2006), the mean number concentration of coarse FBAPs was $\sim 3 \times 10^{-2}$ cm^{-3}, corresponding to ~4% of total coarse particle number. The mean mass concentration of FBAPs was ~1 µg m^{-3}, corresponding to ~20% of total coarse particle mass. The FBAP number size distributions exhibited alternating patterns with peaks at various diameters. A pronounced peak at ~3 µm was essentially always observed and can be described by the following campaign-average lognormal fit parameters: geometric mean diameter 3.2 µm, geometric standard deviation 1.3, number concentration 1.6×10^{-2} cm^{-3}. This peak is likely due to fungal spores or agglomerated bacteria, and it exhibited a pronounced diel cycle with maximum intensity during early/mid-morning. FBAP peaks around ~1.5 µm, ~5 µm, and ~13 µm were also observed, but less pronounced and less frequent. These may be explained by single bacterial cells, larger fungal spores, and pollen grains, respectively.

The observed number concentrations and characteristic sizes of FBAPs are consistent with microscopic, biological and chemical analyses of PBAPs in aerosol filter samples. To our knowledge, however, this study reporting: continuous online measurements of bioaerosol particles over several months, a range of characteristic size

ACPD

9, 17705–17751, 2009

distribution patterns, and a persistent bioaerosol peak at ~3 µm. The measurement results confirm that PBAPs account for a substantial proportion of coarse aerosol particle number and mass in continental boundary layer air. Moreover, they suggest that the number concentration of viable bioparticles is dominated by fungal spores or agglomerated bacteria with aerodynamic diameters around 3 µm rather than single bacterial cells with diameters around 1 µm.

1 Introduction

Biogenic aerosols are ubiquitous in the Earth's atmosphere and they play important roles in atmospheric chemical and physical processes, climate, biological systems, and public health (Cox and Wathes, 1995; Pöschl, 2005; Jaenicke et al., 2007). Primary biological aerosol particles (PBAPs) are pieces of biological material emitted or suspended directly from the biosphere to the atmosphere. The main types and characteristic size ranges of PBAP are viruses (0.01–0.3 µm), bacteria (0.1–10 µm), fungal and fern spores (1–30 µm), plant pollen (10–100 µm), and fragments of animal and plant matter (e.g. Gregory, 1978; Simoneit and Mazurek, 1982; Matthias-Maser and Jaenicke, 1995; Jones and Harrison, 2004; Jaenicke, 2005; Elbert et al., 2007; Bauer et al., 2008). PBAPs can play an important role in public health by affecting allergies (Linskens and Cresti, 2000; Franze et al., 2005) and spreading disease to humans and crops, both naturally and as agents of terrorism (e.g. Lacey and Dutkiewicz, 1994; Brown and Hovmoller, 2002; Ho and Duncan, 2005). Many organisms rely on bioaerosols for the distribution and transfer of genetic material for reproductive purposes, as in the cases of plant pollen and fungal spores, which can also undergo transport over long distances (Elbert et al., 2007, and referencse therein). PBAPs may also influence climate and the hydrological cycle by initiating the formation of clouds and precipitation as cloud condensation and ice nuclei (Dingle, 1966; Schnell and Vali, 1972; Hamilton and Lenton, 1998; Lohmann and Feichter, 2005; Dusek et al., 2006; McFiggans et al., 2006; Sun and Ariya, 2006; Christner et al., 2008; Mortazavi et al.,

ACPD
9, 17705–17751, 2009

2008; Rosenfeld et al., 2008; Ariya et al., 2009; Bowers et al., 2009; Pratt et al., 2009; Prenni et al., 2009).

Recent studies have found significant concentrations of DNA (ng m^{-3}) and a wide range of bacteria and fungal spores in fine and coarse particulate matter from urban, rural, and high-alpine air (Despres et al., 2007; Frölich-Nowoisky et al., 2009). For tropical rainforest regions where both physicochemical processes in the atmosphere and biological activity at the Earth's surface are particularly intense, Elbert et al. (2007) reported that fungal spores account for large fractions of coarse particle mass concentrations (~30%) and estimated global emission rates of the order of 50 Tg a^{-1}. Jaenicke et al. (2007) summarize measurements covering a variety of geographical locations and particle size ranges showing that 15–74% of the total aerosol number as being PBAPs including ~20% in the semi-urban setting in Mainz, Germany (Matthias-Maser and Jaenicke, 1995; Kenny and Jennings, 1998; Gruber et al., 1999; Graham et al., 2003; Wiedinmyer et al., 2009). Continuous measurements of PBAP data have been limited, however, and so actual abundances, properties, as well as the origin of PBAPs and their components are still poorly quantified and understood. Recent model studies and literature reviews highlight the need for more measurement data to constrain regional and global emissions, transport, and abundance of PBAPs in the atmosphere (Burrows et al., 2009a, b; Heald and Spracklen, 2009).

In the past, most PBAP measurements were based on off-line techniques with low time resolution (hours/days). Recently, the application of ultraviolet fluorescence to online aerosol analysis has allowed the detection of PBAPs in real-time, with time resolution of minutes or less (Hairston et al., 1997; Kaye et al., 2005; Gabey et al., 2009). The ultraviolet aerodynamic particle sizer (UV-APS), also known as fluorescent APS (FLAPS), was first developed to quickly detect bioaerosols as possible agents of terrorism, and a detailed description of the instrument used in this study has been given previously (Hairston et al., 1997; Brosseau et al., 2000). Excitation at 355 nm and detection of fluorescence at 420–575 nm are characteristic for reduced pyridine nucleotides (e.g. NAD(P)H) and for riboflavin, which are specific for living cells. Thus,

ACPD
9, 17705–17751, 2009

detection of fluorescence under these conditions indicates the presence of viable biological material in the aerosol particles (Eng et al., 1989; Kell et al., 1991; Li et al., 1991; Hairston et al., 1997). Ho et al. (2002) showed that fluorescence signals from atmospheric aerosols are dominated by PBAPs, and there are no indications that inorganic materials contribute to aerosol fluorescence at the wavelengths used. Non-viable organic material such as nutrient broth and peptone water can also exhibit fluorescence in the operating wavelengths (Agranovski et al., 2003b). These substances are not likely to occur in the atmosphere, however, and if so they would most likely be of biological origin (albeit not viable) and thus qualify as components of PBAPs. Environmental stress has been found to reduce the fluorescence of biological organisms, and the fluorescence signals of NAD(P)H can be influenced by binding to proteins (Huber et al., 2000; Agranovski et al., 2003a). Further investigation will be required to achieve full understanding of the response of the UV-APS to different types of biogenic aerosol particles and to quantify potential interferences with non-biogenic particles and particle components (e.g. soot and polycyclic aromatic compounds, PAHs) that also display fluorescence. As discussed below, such interferences may indeed influence the measurement results obtained for fine aerosol particles (<1 µm). Nevertheless, all available information suggests that coarse fluorescent particles (>1 µm) measured by the UV-APS can be regarded as "fluorescent biological aerosol particles" (FBAP) or viable bioparticles, respectively, and that their abundance represents a lower limit for the actual abundance of primary biological aerosol particles.

Previous work has characterized the UV-APS in the laboratory with respect to aerosols containing marker biological molecules (Agranovski et al., 2004b; Agranovski and Ristovski, 2005), and also with respect to real-time measurement of bacteria (Brosseau et al., 2000; Agranovski et al., 2003a, b) and fungal spores (Kanaani et al., 2007, 2008a, b), but little has been done to utilize the instrument for longer term ambient measurement. A variety of bioaerosol detection techniques have been utilized to characterize bioaerosol emissions from a variety of occupationally specific exposure environments, such as from livestock facilities (Agranovski et al., 2004a; Seedorf, 2004;

ACPD
9, 17705–17751, 2009

Kim et al., 2007), waste treatment plants (Lavoie et al., 2006; Nikaeen et al., 2009) and in various indoor environments (Burge, 1990; Moschandreas et al., 1996; Law et al., 2001). Recently, first fluorescence measurements of bioparticles have been reported for tropical rainforest air (Gabey et al., 2009).

In this study we have applied a UV-APS for the detection and sizing of FBAPs in urban and rural continental aerosols over a four-month period from 3 August–4 December 2006. To our knowledge, this represents the first multi-month ambient measurement study involving an instrument for real-time bioaerosol detection using fluorescence and also the first in a semi-urban environment.

2 Methods

2.1 UV-APS operating principles and conditions

An ultraviolet aerodynamic particle sizer (UV-APS; TSI Inc. Model 3314, St. Paul, MN) was utilized for this study following standard, manual-advised procedures. Aerodynamic particle sizing in the diameter range (D_a) of 0.54–19.81 µm (geometric mid-point diameter) is performed in the instrument by measuring the time of flight between two red (633 nm) He-Ne lasers. Fluorescence of aerosol particles in the wavelength range of 420–575 nm is measured after excitation by a third ultraviolet laser at 355 nm. The particle counting efficiency of the instrument drops below unity at D_a<0.7 µm (counting efficiency ~0.5 at 0.54 µm). Thus, concentration values reported for particles <0.7 µm should be considered as lower limit values. The instrument manufacturer specifies the upper size limit of the UV-APS at 15 µm. Upon manufacturer calibration, however, polystyrene latex spheres (PSL, Duke Scientific) up to 20 µm, were properly sized by the UV-APS, though possibly with lower efficiency. As a result, particles detected between 15–20 µm are included in our analyses, but the reported concentration values should again be considered as lower limit values. Aerosol sampling was performed with a volumetric flow of 5 L min^{-1} (Lpm) at ambient pressure and temperature. Within

ACPD
9, 17705–17751, 2009

the instrument, the total flow was split into an inner sample flow of 1.0±0.1 Lpm passing through the nozzle and optical measurement cell and a sheath flow of 4.0±0.1 Lpm (pressure difference feedback control). The flow rates were regularly checked with external flow meters (TSI Inc. Model 4140 Thermal Mass Flowmeter and Sensidyne Gilibrator-2). The inner and total volumetric flow rates stayed generally within the range of 1.0–1.1 Lpm and 4.9–5.0 Lpm, respectively. In the course of long term operation, a "Check Flow" signal on the instrument occasionally indicated that the actual flow rates exceeded the specified range. In such instances, the inner flow was found to have increased up to ∼1.25 Lpm, while the total flow remained in the range 4.9–5.0 Lpm. The desired flow rates were re-established by cleaning the APS nozzle with compressed air.

The instrument was controlled and the measurement data were recorded with an external computer connected via RS-232 ports using the manufacturer's Aerosol Instrument Manager software (TSI AIM). Measurements were initiated every 5 min and integrated over a sample length of 299 s. Aerodynamic diameter, side scatter intensity, and fluorescence intensity were measured for every detected particle, and results of every 5 min measurement bin were stored in individual sample data files (TSI *.A12 file format). The format and processing of the measurement data is described below. Five-minute sample measurements were continuously repeated over a period of four months from 3 August to 4 December, 2006 (122 days, 34 270 data points) and only briefly interrupted for maintenance procedures (usually less than 30 min per week for flow check and nozzle cleaning as detailed in the instrument manual). The local time (LT) used for data analysis and plotting refers to Central European Summer Time (CEST) from the beginning of the reported measurements in August until 29 October and thereafter to Central European Time (CET). All times reported here are listed as LT.

2.2 Measurement location and sampling

The UV-APS instrument was operated in a laboratory on the third (top) floor of the Max Planck Institute for Chemistry (∼10 m above ground; building N, room 408, eastward-

ACPD
9, 17705–17751, 2009

facing location), which is located on the campus of the Johannes Gutenberg University in Mainz, Germany (49° 59′ 31.07″ N, 8° 14′ 14.64″ E; 100 m a. s. l.). Towards the north and east, the university campus is surrounded by the city of Mainz and adjacent urban areas in the Rhine-Main metropolitan region. Towards the south and west, the university campus is surrounded by farm, grass, and forested land with small villages and towns in a rural region extending over several hundred kilometres. Thus, air masses advected to the sampling locating during this study can be considered as typical central European mixtures of air from a metropolitan area and from a rural background region.

Inside the laboratory, the UV-APS instrument was placed next to a window, through which ambient air was sampled using electrically-conductive silicon rubber tubing (length 1.6 m, inner diameter 12 mm, sample flow residence time 2 s). Flow through the tube was considered laminar at all times, and so diffusion losses are considered negligible for all sampled particle sizes. From the instrument inlet on top of the UV-APS the sampling tube was smoothly bent through the window to minimize particle losses due to impaction (curvature radius ∼1 m), where it terminated facing down and outward (∼45°), about 30 cm off the wall. It is possible that the sampled air masses were influenced by dynamics involving the building structure, though no evidence of this was observed. Additionally, the sampling efficiency of large particles may have been influenced at the sampling tube inlet (especially at high wind velocities). Nevertheless, the frequent observation of large particles (up to 20 µm in diameter) and the variability and consistency of the measurement data presented and discussed below confirm that the measurement results are not governed by the sampling conditions but characteristic for different types of ambient air advected to the measurement location.

2.3 Data processing

2.3.1 Data files and format

Based on the time-of-flight measurement, particles detected by the UV-APS are binned in 52 size channels within the instrument electronics, which are loga-

ACPD
9, 17705–17751, 2009

rithmically scaled with the lower cut-off and geometric mean diameters listed in supplemental Table S1 (see http://www.atmos-chem-phys-discuss.net/9/17705/2009/acpd-9-17705-2009-supplement.pdf). The geometric width of the size channels, $\mathrm{dlog}D_a$, was 0.25 for the lowermost channel (<0.54 µm) and 0.03125 for all other 51 channels (up to 19.81 µm). For each detected particle, the fluorescence intensity measured after the aerodynamic sizing was recorded on a relative scale of 64 channels, ranging from non-detectable (channel 1) to maximum (channel 64) fluorescence signal. The fluorescence intensity detector was used as adjusted and delivered by the manufacturer and tested upon instrument setup with fluorescent polystyrene latex particles (0.5 µm, TSI p/n 2609 053). A typical multi-point size calibration curve for particles <3.5 µm is shown in Fig. S1. Absolute fluorescence intensity data are not recorded by the UV-APS, and the instrument is not calibrated for quantitative number concentration detection.

The TSI AIM software was used to export the correlated data of particle number concentration ($\mathrm{d}N/\mathrm{dlog}D_a$) and fluorescence versus aerodynamic diameter for each 5 min measurement from the original data file (TSI *.A12 format) into an ASCII text file (*.txt format with comma delimiter). Further processing, statistical analysis, and plotting of the data were performed with Igor software (Wavemetrics Inc., Version 6.0.5.0). A user-written Igor program was used to sum $\mathrm{d}N/\mathrm{dlog}D_a$ into two-dimensional matrices of particle size vs. measurement date and time for further analysis. Lognormal fits were performed with the standard fitting algorithm of Igor [fit parameters: x0=D_g, width=$2.303\cdot\sqrt{2}\log\sigma_g$, A=$2.303\cdot N/(\sqrt{\pi}\cdot\mathrm{width})$].

2.3.2 Calculation of FBAP and total particle concentrations

Recently, Kanaani et al. (2007) suggested that all particles recorded by the UV-APS in fluorescence channels 2–64 can be regarded as viable aerosol particles. Agranovski et al. (2004b), however, suggested that non-fluorescent and non-viable particles may be erroneously recorded in fluorescence channel 2. In the present study we calculated

ACPD
9, 17705–17751, 2009

number size distributions of fluorescent aerosol particles, $dN_F/d\log D_a$, for each size bin from the sum of the particle number concentrations from fluorescence channels 3–64, and we calculated the total particle size distributions $dN_T/d\log D_a$, from channels 1–64. For comparison we also calculated $dN_F/d\log D_a$ using channels 2–64 as illustrated in supplemental Figs. S2–S4. These show the enhancement of $dN_F/d\log D_a$ is strongly size dependent (Fig. S4), decreasing from a factor of 3.4 at 0.6 µm to a factor of 1.1 at 20 µm. As a result, by excluding fluorescence channel 2 we expect to obtain a conservative estimate and avoid over-counting the abundance of FBAPs, which in turn can be regarded as a lower limit for the atmospheric abundance of viable PBAPs. The integrated number concentration of coarse fluorescent particles ($N_{F,c}$, >1 µm) is on average 1.5 times higher than the integrated $N_{F,c}$ excluding fluorescence channel 2 (Fig. S3a).

Some fraction of non-biological aerosol particles, including soot and PAHs, exhibit fluorescence and can be erroneously counted as FBAPs by this technique. This is most likely to occur at small (<1 µm) particle sizes where contribution from anthropogenic particles from combustion sources is dominant. If, for example, only a very small amount (e.g. 0.1%) of a non-biological particle mode with peak of 100 cm^{-3} at 0.75 µm exhibited fluorescence, a peak of 0.1 cm^{-3} would appear in the fluorescent particle number distribution. This peak may often be large enough to appear as a distinct peak in the distribution of fluorescent particles (Sect. 3.2). To investigate the contribution of non-biological particles that are counted by this technique (only considering fluorescence channels >3) the correlations between the integrated number concentrations of fluorescent particles (N_F) and total particles (N_T) were plotted separately for particles less than 1.0 µm and greater than 1.0 µm (Fig. S5). The correlation of the sub-µm particles is systematically linear (R^2=0.51, 34 270 data points), with most outliers grouped as individual particle events, whereas the correlation of the supermicron particles is more random (R^2=0.17). Viable biological particles are likely to have different sources and suspension mechanisms from the majority of the anthropogenic source-dominated sub-µm particles observed in this semi-urban location. As a result,

correlation of N_F with N_T indicates that a large percentage of particles exhibiting fluorescence may be from anthropogenic sources as is the case for sub-µm particles, but not for supermicron particles. Similar correlations were also performed for smaller cut sizes. Goodness of fit values for these correlations increased with decreasing cut size, indicating an increasing influence of anthropogenic sources (e.g., Fig. S6 with R^2=0.86 for particles <0.723 mm).

To avoid/minimize interference with non-biological fluorescent particles and for simplicity, we focus our analysis on coarse particles (>1 µm), and we exclude particles <1 µm from the discussion of integral number concentrations. Accordingly, we take the integral number concentration of fluorescent particles larger than 1 µm, $N_{F,c}$, as the concentration of coarse FBAP. Similarly, $N_{T,c}$ refers to the total integral number concentration of particles detected by the UV-APS larger than 1 µm. Particle mass size distributions ($dM/d\log D_a$) were calculated for each size channel by multiplication of $dN/d\log D_a$ with the volume of an aerodynamically equivalent sphere with the geometric midpoint diameter ($D_{a,g}$) assuming a density of 1 g cm^{-3} and a shape factor of 1. Integral mass concentrations of coarse FBAPs ($M_{F,c}$) and total coarse particles ($M_{T,c}$) were also calculated by integration of particle mass >1 µm.

2.4 Detection limits

For the interpretation and scaling of size distribution data and plots (Sect. 3.2) we have calculated the lowest detectable concentrations (LDC) measurable in each size channel of the UV-APS during the 5 min sample measurements performed in this study. For the incremental particle number concentration per size channel (dN) as well as for the integrated particle number concentration (N), the LDC is given by the inverse of the sample volume passing through the measurement cell: $LDC_N = LDC_{dN} = 2\times10^{-4}$ cm^{-3}. With regard to size distributions, the lowest detectable value is given by division of LDC_{dN} through the geometric width of the size channel: $LDC_{dN/d\log D_a} = 8\times10^{-4}$ cm^{-3} for channel 1 (<0.54 µm, $d\log D_a$=0.25) and $LDC_{dN/d\log D_a} = 6.4\times10^{-3}$ cm^{-3} for size chan-

ACPD
9, 17705–17751, 2009

nels 2–52 (0.54–19.81 µm, dlogD_a=0.03125), used for further analysis.

The LDC of particle mass scales with the third power of the aerodynamic diameter of detected particles. For each size channel LDC_{dM} has been calculated by multiplication of LDC_{dN} with the volume of the aerodynamic equivalent sphere with geometric midpoint diameter ($D_{a,g}$) and density of 1 g cm^{-3}. The values of LDC_{dM} are listed in Table S1, ranging from 3 pg m^{-3} (channel 1) to 0.8 µg m^{-3} (channel 52). The corresponding values of $LDC_{dM/dlogD_a}$ range from 11 pg m^{-3} to 26 µg m^{-3}. The lowest detectable integrated mass concentration, LDC_M, is effectively given by the lowest value of LDC_{dM} in the range of size channels which have been used for data analysis in this study (channels 2–52): 17 pg m^{-3}. The LDC values are the same for FBAPs and total aerosol particles (TAPs, including non-fluorescent aerosol particles) and are listed here for individual measurements at the conditions of this study. The LDC of data points averaged over a longer time period will scale inversely with the number of measurements recorded (n). Note that all particle sizes given here are $D_{a,g}$, but will be simplified as D_a.

3 Results and discussion

3.1 Particle number and mass concentrations

3.1.1 Overview of number concentrations

To our knowledge, no other time series of bioaerosol measurements with similarly high time resolution extending over a similarly long period have been previously reported. Thus, we first outline characteristic features of the time series (Figs. 1–2) in a general way to help the reader gain an overview of the observed concentration levels, trends, and variability before moving on to a more formal statistical treatment of the data (Fig. 3) and more detailed size-resolved analysis. Figure 1 shows the number concentration of fluorescent biological aerosol particles measured with the UV-APS for each 5 min period as time series of size-resolved measurements (dN_F/dlogD_a), inte-

ACPD
9, 17705–17751, 2009

grated total coarse FBAP number ($N_{F,c}$), and as a number ratio of integrated coarse FBAP to TAP ($N_{F,c}/N_{T,c}$). Figures similar to Fig. 1, each with a range of one month are shown in Fig. 2 in order to view temporal trends with more precision.

Through-out the measurement period the total coarse particle number concentration, $N_{T,c}$, varied mostly within a relatively narrow range of values between 0.37–1.30 cm^{-3} (25–75th percentiles), but also exhibited highly variable large spikes and strong diurnal and day-to-day variations frequently exceeding one order of magnitude between adjacent days (supplemental Figs. S7–S8). Background concentrations consistently dropped to <0.4 cm^{-3} between morning peaks during most of the campaign. The highest total particle number concentrations were observed in November, with daily peaks above 8 cm^{-3} and maxima up to 14 cm^{-3} during 27 November–2 December. Several events of high $N_{T,c}$ maxima (>4 cm^{-3}) and high sustained $N_{T,c}$ background (>2 cm^{-3}) also occurred between 11 October–13 November, with the largest occurring the early mornings of 30 October and 1 November. The lowest values of $N_{T,c}$ were detected 13–14 November, with minima as low as 0.03 cm^{-3}.

In contrast to total particles, the FBAP number concentration, $N_{F,c}$, exhibited less pronounced spikes and showed more consistent diel and day-to-day behavior (Figs. 1a and 3b; 0.012–0.033, 25–75th percentiles). The highest $N_{F,c}$ concentrations were observed 25–27, 30–31 October and 8 November, with maxima up to 0.85 cm^{-3} and >0.3 cm^{-3} each day. The lowest sustained (>6 h) values of $N_{F,c}$ were detected on 2 and 13 November when the concentration dropped to 0.0015 cm^{-3} and remained below ~0.005 cm^{-3} for 8 and 16 h, respectively. This period coincides with a several day period of high $N_{T,c}$. The relative contribution of FBAP to TAP number, $N_{F,c}/N_{T,c}$, showed similar temporal behaviour to $N_{F,c}$, but with more pronounced extremes due to the variability of the total number of coarse particles. $N_{F,c}/N_{T,c}$ varied typically in the range of 1.7–5.5% (25–75th percentiles). The highest consistent FBAP fractions were observed 12–19 August, where maxima exceeded 12% each day and 23% at several points. Other consistently high (>5%) $N_{F,c}/N_{T,c}$ periods were observed 20–27 October and 14–19 November. In general, $N_{T,c}$ and the $N_{F,c}$ fraction of total coarse particles

ACPD
9, 17705–17751, 2009

are inversely correlated, but with a high amount of scatter; as $N_{T,c}$ increases, $N_{F,c}/N_{T,c}$ decreases.

The statistical distribution of 5 min number concentration measurements over the course of the campaign are shown in Fig. 3 and tabulated in Table 1. The monthly mean of $N_{T,c}$ varied by a factor of ~3 over the course of the measurement period, from a minimum in September to a maximum in November. The months of October and November showed not only higher mean $N_{T,c}$ values, but also higher relative variability, reflected in the size of the 5–95th percentile bars in Fig. 3. The mean values of $N_{F,c}$ showed more consistency, however. September's low $N_{F,c}$ (0.018 cm^{-3}) was the only monthly mean value outside the relatively narrow range of 0.026–0.032 cm^{-3}.

Diel (24-h) trends over the four-month measurement period were also analyzed. Figure 4 shows plots similar to Fig. 1, but showing campaign median values for each hour of the day. A daily $N_{F,c}$ peak of 0.029 cm^{-3} at 07:00 LT is clearly evident above a relatively flat background of 0.017–0.018 cm^{-3} (Fig. 4a). $N_{F,c}/N_{T,c}$ shows a similar trend, with a peak at 07:00 of 4.4% above an early morning background of 2.6%. A second, minor peak of 3.9% in the FBAP coarse particle number ratio is evident at 17:00. This is a result of the corresponding decrease in $N_{T,c}$ at this time, while the $N_{F,c}$ is relatively constant. Figure 4b shows that the 07:00 peak in $N_{F,c}$ is a result of a peak in $dN_F/d\log D_a$ at 3.2 µm. The peak at this size is the most prominent particle size through all hours of the day, but increases at night and is highest in the mid-morning (05:00–10:00). Figure 5 shows the same diel plot, with each panel showing median values for one of the four individual months of the measurement period. This further highlights the consistency of the ~3 µm $N_{F,c}$ peak. In each plot of monthly median values the ~3 µm peak is dominant at all times of the day, but retains a diel cycle with a peak in the mid-morning. Of the four months of $N_{F,c}$ measurements, August exhibits the highest diel peak at 0.040 cm^{-3} during 07:00–08:00, as well as the largest relative diel swing (×3.5 between diel minimum and maximum). September, however, showed relatively little diel swing in $N_{F,c}$ (×1.6) and the lowest diel peak of any month (0.019 cm^{-3}). The November pattern was unique, however, because the ~3 µm peak shows two distinct

ACPD
9, 17705–17751, 2009

diel maxima at 07:00 and 15:00. $N_{F,c}$ shows two peaks with relatively equal height (0.025 and 0.028 cm^{-3}, respectively) caused by the increased concentration of ~3 µm particles. $N_{F,c}$ then drops off steeply after 15:00 and rises steeply again immediately before 07:00. The November pattern also shows a more prominent peak at ~0.8 µm during night time hours that is not as clearly seen in the other months. Size distributions for selected periods will be discussed in detail in Sect. 3.2.

Diel plots of $N_{T,c}$ are shown as an average for the campaign and for each month in supplemental Figs. S9–S10, respectively. The size-resolved $dN_T/dlogD_a$ (lower panels) over the four months of measurement consistently shows a dominant peak at <1.0 µm during night-time hours. The maxima of $dN_T/dlogD_a$ during August and September occurred at 04:00, while the peak shifted increasingly earlier in October and November to 02:00 and 21:00, respectively (a second peak in September is also observed at 09:00). The diel cycles of TAPs in (semi-)urban environments are usually governed by boundary layer mixing effects and anthropogenic emissions (Garland et al., 2008, 2009). The diel cycles of FBAPs, however, are clearly different from those of TAP sources, and variability of FBAP sources seems to dominate over boundary layer mixing effects. Steep increase in FBAP concentrations observed in the morning after sunrise (~06:00 in August–~08:00 in December) may suggest that a combination of high relative humidity and sunlight enhances the emission from bioaerosol sources (Elbert et al., 2007). Correlations of meteorological parameters with TAP and FBAP were performed and show a qualitative increase in $N_{F,c}$ with relative humidity, but with variable time offset and low correlation coefficient. No statistically significant correlation was found with wind direction. Further statistical analysis will be performed in follow-up studies, but are beyond the scope of this work.

Overall, the results show that FBAPs account for a small but significant fraction (typically ~3–4%, at most ~15%) of total coarse aerosol particle number in the investigated size range (1–20 µm), and they indicate that the sources and sinks of FBAPs are less variable than those of other types of aerosol particles in central Europe. These findings support earlier suggestions that bioaerosols may be regarded as the natu-

ACPD
9, 17705–17751, 2009

ral background aerosol over vegetated continental regions (Jaenicke, 2005; Andreae, 2007; Jaenicke et al., 2007; Andreae and Rosenfeld, 2008; Martin et al., 2009).

3.1.2 Overview of mass concentrations

We also present here an overview of the estimated FBAP mass concentration over the course of the measurement period. Figure 6 shows the integrated total coarse particle mass ($M_{F,c}$), the fraction of integrated FBAP mass to TAP mass ($M_{F,c}/M_{T,c}$), as well as a time series of size-resolved measurements ($dM_F/d\log D_a$). Figures similar to Fig. 6, each with a range of one month are shown in supplemental Fig. S11 in order to view temporal trends with more precision.

$M_{T,c}$ (Figs. S12–S13) exhibited a pattern of large fluctuations and frequent (several times per week) large peaks (>25 $\mu g\,m^{-3}$) on top of a relatively clean background of between 1–4 $\mu g\,m^{-3}$. The highest peaks came during a period from 25–27 October when daily morning maxima exceeded 100 $\mu g\,m^{-3}$ each day and reached 270 $\mu g\,m^{-3}$on 26 October. The periods from 28 August–1 September and 6–7 September also exhibited high daily $M_{T,c}$ peaks of >45 $\mu g\,m^{-3}$. 2–3 October and 13–14 November exhibited the lowest $M_{T,c}$ values at <1 $\mu g\,m^{-3}$ for ~12, 24 h, respectively and daily minima regularly dropped to <1.5 $\mu g\,m^{-3}$ over the course of the measurement period. $M_{F,c}$ varied at constant background of 0.51–1.49 $\mu g\,m^{-3}$ (25–75th percentiles), also with frequent spikes in concentration. The highest background concentration rose 9–28 October when levels rarely dropped below 0.8 $\mu g\,m^{-3}$ and peaked >40 $\mu g\,m^{-3}$ at least daily from 25–27 October. Temporal trends in $M_{F,c}$ are only poorly reflected in $M_{F,c}/M_{T,c}$ temporal behavior, as the ratio is qualitatively dominated by $M_{T,c}$. The fraction of FBAP to TAP coarse particle mass varied within a range of 11–27% $\mu g\,m^{-3}$ (25–75th percentiles) over the course of the measurements. Events with very high FBAP mass fractions above 65% occurred at least once a month (peaking at 92% on 9 August) and >70% six times.

The statistical distribution of five-minute mass concentration measurements over the course of the campaign are shown in Fig. 7 and tabulated in Table 1. The monthly

ACPD
9, 17705–17751, 2009

mean values of $M_{T,c}$ exhibited lower relative variability, but similar temporal trends as $N_{T,c}$, with a general increase through the course of the measurement months. Monthly mean $M_{T,c}$ values varied by a factor of ~1.5 from a minimum of 5.3 µg m^{-3} in August to 8.2µg m^{-3} in November. The 95th percentile values were 2.1–2.3 times higher than the mean values of $M_{T,c}$ in each case. The monthly mean values of $M_{F,c}$ showed similar relative variability as $M_{T,c}$ and $M_{F,c}$, except in October when both mean $M_{F,c}$ values and relative variability were significantly higher. The mean value of $M_{F,c}$ (1.9 µg m^{-3}) in October represents the only month above the range of 0.92–1.1 µg m^{-3}. Similar to the trend in $N_{F,c}/N_{T,c}$, $M_{F,c}/M_{T,c}$ shows a gradual decrease over the course of the four months measured, with high $M_{F,c}$ in October causing the only outlier. The mean values are only marginally higher than the median values for $M_{F,c}/M_{T,c}$, indicating relatively low temporal variability. The median and mean for $M_{F,c}/M_{T,c}$ over the course of the campaign were 18.5 and 19.5%, respectively. On average, the relative contribution of FBAP to TAP coarse particle mass was ~5 times larger than the contribution of FBAP to TAP coarse particle number (~3.9%). This is consistent with the observation that FBAPs show enhanced prevalence among large aerosol particles (3–10 µm), as shown and discussed in Sect. 3.2.

Diel trends in $M_{F,c}$ were also analyzed and are shown in Fig. 8 for the entire campaign and in supplemental Fig. S14 for each individual month. Figure 8a shows that the lowest $M_{F,c}$ values occurred at night, with a temporally broad increase in $M_{F,c}$ from ~05:00–14:00 and a maximum at 08:00 (1.17 µg m^{-3}). The overall trend of night-time lows with peak in mid-morning is similar to diel $N_{F,c}$ trend, but $M_{F,c}$ shows a greater relative increase from diel minimum to maximum compared with $N_{F,c}$ (66% and 79%, respectively), and the morning $M_{F,c}$ peak is temporally broader and extends later in the day. $M_{F,c}/M_{T,c}$ exhibited a temporal trend similar to $M_{F,c}$, but less pronounced and showed relatively minor diel variability (minimum 14.7%, maximum 20.5%). The size-resolved diel trend of $M_F/\mathrm{dlog}D_a$ was also similar to $N_F/\mathrm{dlog}D_a$ in that a mid-morning peak of intermediate size (~5 µm for particle mass distribution) heavily influences the

ACPD
9, 17705–17751, 2009

trend in overall integrated coarse particle mass. Though relatively few in particle number, particles between 7–9 µm are consistent through day-light hours (~07:00–17:00), however, and are the largest contributors to $M_{F,c}$ at those times. $M_{F,c}$ for August (Fig. S14a) shows the clearest morning peak compared to the other three months, but also shows relatively little diel cycle in $M_{F,c}/M_{T,c}$ (18.0% minimum, 22.0% maximum). As was also the case for $N_F/\mathrm{dlog}D_a$, an afternoon peak of intermediate particle diameter became more apparent as each month progressed. The contribution of mass by the larger particles (7–9 µm) is most significant in September and November, and least significant in August. During all periods of investigation particles smaller than 3 µm, though often important in number, were negligible in terms of particle mass.

3.2 Size-distributions of particle number and mass

3.2.1 Exemplary particle size distributions

Figure 1b shows that FBAPs with $D_a \approx 3$ µm were nearly ubiquitous during the campaign. The FBAP peak at ~3 µm exhibits a clear diel cycle (Fig. 4b), but rarely disappears completely. In addition to this peak, a variety of other FBAP peaks were frequently observed for varying lengths of time. Out of a wide range of different patterns and peaks in $\mathrm{d}N_F/\mathrm{dlog}D_a$ observed during the campaign, four characteristic modes of FBAP were most commonly found and clearly distinguishable. The peak diameters of these modes were typically around ~1.5 µm, ~3 µm, ~5 µm, ~13 µm, respectively. In the following we highlight exemplary periods and size distributions illustrating characteristic features and the variability of the most commonly observed patterns and peaks in $\mathrm{d}N_F/\mathrm{dlog}D_a$.

Figure 9a–b (exemplary period # 1) illustrate the most frequently observed individual peaks in the $\mathrm{d}N_F/\mathrm{dlog}D_a$ distribution, with maxima at 3 µm and 0.7 µm. As discussed in Sect. 2.3.2, the sub-µm peak in $\mathrm{d}N_F/\mathrm{dlog}D_a$ is likely due to fluorescent particle components from anthropogenic sources (soot/PAHs from combustion sources). As shown in the online supplement (Fig. S15), the total aerosol particle distribution $\mathrm{d}N_T/\mathrm{dlog}D_a$

ACPD
9, 17705–17751, 2009

observed during exemplary period #1 exhibits a much higher peak at the same diameter, and the ratio between $dN_F/d\log D_a$ and $dN_T/d\log D_a$ at D_a=0.7 µm is similar to the near-constant proportion of fluorescent sub-µm particles observed throughout the campaign (~0.1%, Fig. S5). Accordingly, we do not consider this and other sub-µm peaks in $dN_F/d\log D_a$ as characteristic for FBAP and exclude them from further analysis and discussion. With regard to the FBAP peak observed at $D_a \approx 3$ µm, period #1 provides a relatively narrow example (nearly monodisperse with $\sigma_g \sim 1.2$) that may consist of particles from the same or similar sources (e.g., spores from similar types of fungi). In many other cases we observed broader peaks that seemed to comprise two or more types of FBAPs with slightly different diameters (Figs. S16–17) or overlapped with other characteristic modes that are like to have originated from different sources and biological species.

Figures 9c–d (exemplary period #2) illustrate another frequently observed FBAP size distribution pattern, with a broad peak centered at ~3 µm and a smaller peak at ~1.5 µm. Periods #1 and #2 both exemplify situations where the observed FBAP size distribution was fairly stable over the course of <12 h, as opposed to events where short-term bursts of FBAPs extended over only a few hours (Figs. 10c–d, S16). Figure 10a–b (exemplary period #3) illustrate a situation where the FBAP mode around ~5 µm was not just overlapping with, but much more pronounced than the ~3 µm mode. In this case the peak near 5 µm is exceptionally narrow, suggesting particles from the same or similar sources as discussed above. In most other cases, the peaks around ~5 µm were broader (Fig. S16) and likely composed of particles from a variety of different sources. Figure 10c–d (exemplary period #4) illustrate a situation where a narrow peak at ~1.1 µm dominates the FBAP size distribution. This pattern was uniquely observed over a 35 min period on 17 August. The small particle size and the short duration suggest that the ~1.1 µm peak consisted of single bacterial cells from a nearby source. It occurred in parallel to a narrow peak at ~3 µm, but the temporal evolution of the two peaks was very different. The peak at ~3 µm was present before and persisted beyond the short-term burst of the 1 µm-sized FBAPs.

ACPD
9, 17705–17751, 2009

Figure 11a–d (exemplary periods #5 and #6) show FBAP size distributions with a distinct and narrow peak at ~13 µm that appeared on 10 October and persisted until 29 October. Most likely the ~13 µm peak is due to pollen grains from a nearby tree that was blossoming during this exceptionally warm period in October 2006. In the relevant size range (12–17 µm), the FBAP peak (pollen grains) also dominated the total aerosol particle concentration and size distribution with FBAP/TAP ratios in the range of 60–100% (25–75th percentile, mean 73%). Figure 11 also shows that the size resolution and sensitivity of the UV-APS are sufficient for separating and quantifying different types of FBAPs independent of the varying concentrations of TAP (and non-biological fluorescent particles <1 µm). Supplemental Fig. S18a–d shows that FBAP peaks around ~1.5 µm, ~3 µm and ~5 µm could be observed, even during periods of very low aerosol concentration levels.

3.2.2 Average size distributions

The number and mass size distributions for both TAPs and FBAPs averaged over the whole campaign are shown in Fig. 12. The TAP number size distribution $dN_T/d\log D_a$ was generally dominated by a peak at the lower end of the investigated size range ($D_a \approx 0.7$ µm, Fig. 12a; monthly averages in Fig. S19). Note that this "peak" is likely due to a steep decrease in the UV-APS detection efficiency for small particles at D_a <0.7 µm; otherwise the distribution would likely increase to the lowest size bin. Supplemental Fig. S20 shows the campaign mean $N_T/d\log D_a$ size distribution with a logarithmic y-axis in order to resolve characteristic features at the low values of $dN_T/d\log D_a$ observed at large diameters. For example, a shoulder at ~3 µm can be attributed to the corresponding FBAP peak in $N_F/d\log D_a$.

The campaign and monthly average size distributions of fluorescent aerosol particles, $dN_F/d\log D_a$, are shown in Figs. 12c and 13a–d, respectively. The sub-µm peak at $D_a \approx 0.7$ µm generally coincided with the peak in $N_T/d\log D_a$ and is not considered characteristic for biological particles as discussed above. The campaign average size distribution was dominated by an FBAP peak at ~3 µm, and in the monthly averaged

ACPD
9, 17705–17751, 2009

size distributions of August and October this peak was even narrower and more intense. In the monthly averaged size distributions of September and November, however, the peak was substantially broader and the maximum was shifted towards higher D_a, indicating the presence of different and more diverse types of FBAP. A small mode at ~1.5 µm is present in the mean FBAP distribution as well as in each monthly plot. Lastly, an FBAP mode at ~13 µm can be seen in the mean FBAP number distribution. As discussed previously, this mode was small in number concentration, but was almost completely comprised of FBAP material.

The size distributions of TAP mass were much broader than those weighted by number and also differed in the fact that they exhibited several more distinct local maxima. The campaign mean TAP mass distributions (Fig. 12b) looked generally similar to each of the constituent months (Fig. S21) with a distinct peak at 0.8 µm, a broad peak with two local maxima centered between 3–8 µm, and an upward slope at particle diameters above ~12 µm. During August, September and November the same four peaks were observed in the TAP mass distribution as in the campaign mean, while in October an additional peak at 13.8 µm was also observed, showing what are likely pollen particles observed during the month of October to be of high enough relative FBAP fraction to contribute noticeably to the monthly TAP mass distribution. The highest concentration at each of the two dominant TAP mass peaks were in November, when the monthly mean was 0.36 and 0.31 µg m^{-3} for the 0.84 and 3.05 µm peaks, respectively.

The campaign mean FBAP mass distribution (Fig. 12d) was generally bimodal , with broad peaks centered at 4.4 and 7.8 µm. A sharper peak centered at 13.8 µm came from the October-specific pollen particles, not as clearly evident in any other month (Fig. S22). The August mean FBAP mass distribution (Fig. S22a) also shows a small shoulder at 13.8 µm, indicating that the source of the October particle peak may have additional sources located farther from the sampling inlet. These may be related to other pollen-producing plants that were releasing FBAPs earlier in the summer. Unlike the TAP mass distributions, the FBAP mass distributions had consistently negative slopes at the highest particle diameter channels, indicating the large particles shown

ACPD
9, 17705–17751, 2009

in the TAP mass distribution were from some mechanical process that did not also produce particles containing measurable concentrations of viable biological material. In general, the size distributions of FBAP mass were shifted to larger particle sizes in September and October as compared with August and November.

3.2.3 Ratio of fluorescent bioparticles to total particles

Taking a ratio of the number of FBAPs (dN_F) and TAPs (dN_T) in each size bin allows the determination of the relative contribution of viable biological particles at each particle size. As discussed previously, the mean shape factor and particle density of each particle were each assumed to have a value of unity. This determines that the value of the $dN_F/dN_{T,c}$ ratio is equal to dM_F/dM_T by definition. For observed particles of diameter less than 2.5 µm, the dN_F/dN_T ratio was less than 10% for an average of the entire measurement period (Fig. 14) and for each individually-averaged month (Fig. S23), indicating that relatively few of these small particles were FBAPs. Mean ratio curves show two local maxima, consistently located at similar particle diameters of 3.8–4.7 µm and 9.0–10.4 µm, respectively. The peaks are more distinct in the August and September averages, while for October and November the mean ratio curves appear closer to being a broad single peak between 3 and 12 µm. In August 32% of the total particles at the distinct peak with an aerodynamic diameter of 4.4 µm were identified to fluoresce and were therefore considered to be FBAPs, while in September the value for the same peak (4.7 µm) dropped slight to 30%, and then decreased further in October (3.8 µm) and November (4.7 µm) to 23% and 24%, respectively. The second peak in the FBAP to TAP ratio that can be clearly seen in each of the four months showed a slightly larger ratio: August (38%, 10.4 µm), September (34%, 9.0 µm), and November (31%, 9.6 µm). The October peak was obscured by an additional large peak at ~13 µm and was therefore more difficult to quantitatively determine. This ~3 week-long particle event resulted in producing a relatively sharp peak at 12.9 µm in the October average, with a ratio of 62% of the particles as being FBAPs. A period from 6–7 August also shows a high percentage (>60%) of FBAP at D_a 11–15 µm, indicating that while the large particle

ACPD
9, 17705–17751, 2009

peak in October was the most pronounced, other periods also indicate FBAPs in this size range. The counting statistics, as discussed in the previous section, are poor for the detection of large particles (>~8 µm), and therefore median values often reflect the fact that particles of this size were often not present in >50% of the sampled 5 L volumes. The mean (red) curve, therefore, best represents the dN_F/dN_T ratios at the upper particle sizes. Further example of this is that the light gray shaded area between the 5th and 95th percentile curves covers the entire ratio from 0–100% at all particle diameters greater than ~7 µm and that the median value goes to zero at ~10 µm for each month.

The ratio of the size distributions averaged over the entire measurement campaign (Fig. 14) show similar trends to each of the individual months. Three local maxima are apparent, at aerodynamic particle diameters of 4.70, 9.65, and 13.8 µm. Though the particles of diameter greater than 13 µm were almost exclusively present within the month of October, the month's large peak at these sizes heavily influences the 4-month average (Fig. 12a). As a way of removing the very local point source during October, the average contribution of FBAP to TAP number and mass over this four-month measurement period was calculated with the period of 10–29 October removed. The ratio plot is shown in Fig. S24 for comparison, and shows a similar pattern to Fig. 14, but without the sharp peak at 13.8 µm.

4 Summary and conclusions

In this study we investigated the capability of a UV-APS operated continuously in Mainz, Germany over the 4-month period of August–November 2006 to quantify the concentration and size of viable biological aerosol particles in urban and rural European continental air. For this purpose, time series of the integrated coarse particle number and mass concentrations as well as particle mass and number size distributions of both total particles and FBAPs from the campaign were analyzed. Great variations in coarse particle number and mass concentrations (1–20 µm) as well as significant temporal

ACPD
9, 17705–17751, 2009

variability of size distributions (using 5-min measurement points) were observed. Over the course of the measurement period the coarse particle number concentration of FBAPs varied in the range of 1.2×10^{-3}–1.4 cm^{-3}, with an arithmetic mean value of 0.027 cm^{-3}(±0.026 cm^{-3}, standard deviation). These accounted for 0.09–67% (mean value 3.9%±2.8%) of the total coarse particle number concentration. The coarse particle mass concentration of FBAPs varied in the range of 4×10^{-3} µg m^{-3} to 123 µgm^{-3}, with an arithmetic mean value of 1.3 µg m^{-3} (±2.0 µg m^{-3}) The coarse particle mass of FBAPs accounted for 0.067–92% (mean value 20%±11%) of total coarse particle mass concentrations.

The TAP size distribution was almost always monomodal, dominated by a peak at ~0.60–0.75 µm, and a peak in the FBAP distribution reflecting nearly identical size and temporal variability characteristics was almost always also present. This peak was likely a result of combustion sources exhibiting spurious fluorescence due to soot and PAHs. After investigating the correlation between small (<1.0 µm) particles exhibiting fluorescence with peaks in the TAP distribution we concluded to exclude particles of aerodynamic diameter less than 1.0 µm in order to avoid overestimation of FBAPs and therefore conservatively estimate FBAPs as the lower limit of ambient, viable PBAPs. Size distributions of remaining FBAPs commonly alternated between periods exhibiting from one to four FBAP peaks. The observed temporal variability of peaks in the FBAP size distribution is not surprising in view of the high diversity and different frequencies of occurrence of bacteria and fungal spores detected by microscopy, cultivation and molecular genetic analyses of air particulate matter (Despres et al., 2007; Elbert et al., 2007; Frölich-Nowoisky et al., 2009). After investigating trends in FBAP size distributions, however, the FBAP peaks can be broadly classified into four FBAP modes. The most common mode was observed around ~3 µm as the dominant FBAP peak. An average of the campaign shows a strong diel cycle to the ~3 µm peak with a maximum in the mid-morning at 07:00 after the sun came up and a constant background throughout the rest of the day. This mode is likely due to fungal spores and their mechanism for release may be some combination of elevated relative humidity and sunlight.

ACPD
9, 17705–17751, 2009

The additional FBAP modes observed over the four months of measurements can be grouped around ~1.5 µm, ~5 µm, and ~13 µm. The smallest mode was likely caused by individual bacterial cells or agglomerates and was most often observed at ~1.5 µm, though the peak of this mode varied between 1.1–1.8 µm. The ~5 µm mode encompasses a variety of peaks observed at different times, though rarely was it seen as a monodisperse peak or set of peaks. Peaks in this region were most often broad and not lognormally distributed, but often distinct from the 3 µm peak. The least commonly observed mode is a ~13 µm peak observed for three weeks in October. Though the peak exhibited low absolute concentration ($<2\times10^{-3}$ cm^{-3}), the relative fraction of FBAP to TAP during this period and size range averaged 73% and often ranged to 100%. These particles were very likely pollen grains released from a nearby blossoming tree. Lognormal fits of selected FBAP peaks were performed in order to provide estimates of characteristic PBAP modes for inputs for aerosol models.

The UV-APS instrument was shown to be capable to detect FBAPs in real-time at concentrations characteristic for ambient air in semi-urban and rural European continental regions. In addition, a sample length of 5-minutes was determined to be adequate for observing fluctuations in the concentrations of TAPs and FBAPs. The determination that FBAP concentration makes up an average of 3.9% of the total coarse aerosol number and 20% of the coarse aerosol mass is significant. Few studies have been able to show the concentration of viable biological aerosol concentrations over an extended sampling period, and to our knowledge this paper represents the first multi-month study that publishes the concentration of these particles in a semi-urban area using a direct technique from real-time, fluorescence detection measurement.

Appendix A

List of frequently used acronyms and symbols

See Table A1.

ACPD
9, 17705–17751, 2009

Acknowledgements. J. A. H. and B. T. contributed equally to this work. This work has been funded by the Max Planck Society, and the authors gratefully acknowledge support by M. O. Andreae, W. Elbert, V. Després, and A. G. Wollny.

The service charges for this open access publication have been covered by the Max Planck Society.

References

Agranovski, V., Ristovski, Z., Hargreaves, M., Blackall, P. J., and Morawska, L.: Performance evaluation of the UVAPS: influence of physiological age of airborne bacteria and bacterial stress, J. Aerosol Sci., 34, 1711–1727, doi:10.1016/s0021-8502(03)00191-5, 2003a.

Agranovski, V., Ristovski, Z., Hargreaves, M., Blackall, P. J., and Morawska, L.: Real-time measurement of bacterial aerosols with the UVAPS: performance evaluation, J. Aerosol Sci., 34, 301–317, doi:10.1016/s0021-8502(02)00181-7, 2003b.

Agranovski, V., Ristovski, Z., Blackall, P. J., and Morawska, L.: Size-selective assessment of airborne particles in swine confinement building with the UVAPS, Atmos. Environ., 38, 3893–3901, doi:10.1016/j.atmosenv.2004.02.058, 2004a.

Agranovski, V., Ristovski, Z. D., Ayoko, G. A., and Morawska, L.: Performance evaluation of the UVAPS in measuring biological aerosols: Fluorescence spectra from NAD(P)H coenzymes and riboflavin, Aerosol Sci. Technol., 38, 354–364, doi:10.1080/02786820490437505, 2004b.

Agranovski, V. and Ristovski, Z. D.: Real-time monitoring of viable bioaerosols: capability of the UVAPS to predict the amount of individual microorganisms in aerosol particles, J. Aerosol Sci., 36, 665–676, doi:10.1016/j.jaerosci.2004.12.005, 2005.

Andreae, M. O.: Aerosols before pollution, Science, 315, 50–51, doi:10.1126/science.1136529, 2007.

Andreae, M. O. and Rosenfeld, D.: Aerosol-cloud-precipitation interactions. Part 1. The nature and sources of cloud-active aerosols, Earth-Sci. Rev., 89, 13–41, doi:10.1016/j.earscirev.2008.03.001, 2008.

Ariya, P. A., Sun, J., Eltouny, N. A., Hudson, E. D., Hayes, C. T., and Kos, G.: Physical and

chemical characterization of bioaerosols – Implications for nucleation processes, Int. Rev. Phys. Chem., 28, 1–32, doi:10.1080/01442350802597438, 2009.
Bauer, H., Schueller, E., Weinke, G., Berger, A., Hitzenberger, R., Marr, I. L., and Puxbaum, H.: Significant contributions of fungal spores to the organic carbon and to the aerosol mass balance of the urban atmospheric aerosol, Atmos. Environ., 42, 5542–5549, doi:10.1016/j.atmosenv.2008.03.019, 2008.
Bowers, R. M., Lauber, C. L., Wiedinmyer, C., Hamady, M., Hallar, A. G., Fall, R., Knight, R., and Fierer, N.: Characterization of Airborne Microbial Communities at a High-Elevation Site and Their Potential To Act as Atmospheric Ice Nuclei, Appl. Environ. Microbiol., 75, 5121–5130, doi:10.1128/AEM.00447-09, 2009.
Brosseau, L. M., Vesley, D., Rice, N., Goodell, K., Nellis, M., and Hairston, P.: Differences in detected fluorescence among several bacterial species measured with a direct-reading particle sizer and fluorescence detector, Aerosol Sci. Technol., 32, 545–558, 2000.
Brown, J. K. M. and Hovmoller, M. S.: Epidemiology – Aerial dispersal of pathogens on the global and continental scales and its impact on plant disease, Science, 297, 537–541, 2002.
Burge, H.: Bioaerosols – Prevalence and Health Effects in the Indoor Environment, J. Allergy Clin. Immunol., 86, 687–701, 1990.
Burrows, S. M., Butler, T., Jöckel, P., Tost, H., Kerkweg, A., Pöschl, U., and Lawrence, M. G.: Bacteria in the global atmosphere – Part 2: Modelling of emissions and transport between different ecosystems, Atmos. Chem. Phys. Discuss., 9, 10829–10881, 2009a, http://www.atmos-chem-phys-discuss.net/9/10829/2009/.
Burrows, S. M., Elbert, W., Lawrence, M. G., and Pöschl, U.: Bacteria in the global atmosphere – Part 1: Review and synthesis of literature data for different ecosystems, Atmos. Chem. Phys. Discuss., 9, 10777–10827, 2009b, http://www.atmos-chem-phys-discuss.net/9/10777/2009/.
Christner, B. C., Morris, C. E., Foreman, C. M., Cai, R. M., and Sands, D. C.: Ubiquity of biological ice nucleators in snowfall, Science, 319, 1214–1214, doi:10.1126/science.1149757, 2008.
Cox, C. S. and Wathes, C. M.: Bioaerosols handbook, Lewis, Boca Raton, 1995.
Després, V. R., Nowoisky, J. F., Klose, M., Conrad, R., Andreae, M. O., and Pöschl, U.: Characterization of primary biogenic aerosol particles in urban, rural, and high-alpine air by DNA sequence and restriction fragment analysis of ribosomal RNA genes, Biogeosciences, 4, 1127–1141, 2007, http://www.biogeosciences.net/4/1127/2007/.

ACPD
9, 17705–17751, 2009

Dingle, A. N.: Pollens as condensation nuclei, J. Rech. Atmosph., 2, 231–237, 1966.
Dusek, U., Frank, G. P., Hildebrandt, L., Curtius, J., Schneider, J., Walter, S., Chand, D., Drewnick, F., Hings, S., Jung, D., Borrmann, S., and Andreae, M. O.: Size matters more than chemistry for cloud-nucleating ability of aerosol particles, Science, 312, 1375–1378, doi:10.1126/science.1125261, 2006.
Elbert, W., Taylor, P. E., Andreae, M. O., and Pöschl, U.: Contribution of fungi to primary biogenic aerosols in the atmosphere: wet and dry discharged spores, carbohydrates, and inorganic ions, Atmos. Chem. Phys., 7, 4569–4588, 2007, http://www.atmos-chem-phys.net/7/4569/2007/.
Eng, J., Lynch, R. M., and Balaban, R. S.: Nicotinamide Adenine Dinucleotide Fluorescence Spectroscopy and Imaging of Isolated Cardiac Myocytes, Biophys. J., 55, 621–630, 1989.
Franze, T., Weller, M. G., Niessner, R., and Pöschl, U.: Protein nitration by polluted air, Environ. Sci. Technol., 39, 1673–1678, doi:10.1021/es0488737, 2005.
Frölich-Nowoisky, J., Pickersgill, D. A., Despres, V. R., and Pöschl, U.: High diversity of fungi in air particulate matter, P. Natl. Acad. Sci. USA, 106, 12814–12819, doi:10.1073/pnas.0811003106, 2009.
Gabey, A., Gallagher, M. W., Whitehead, J., Dorsey, J., Burgess, R., Kaye, P. H., Stanley, W., and Ulanowski, Z.: Real-time Observations of Fungal Spore Number in a Malaysian Tropical Rain Forest, Biotropica, accepted, 2009.
Garland, R. M., Yang, H., Schmid, O., Rose, D., Nowak, A., Achtert, P., Wiedensohler, A., Takegawa, N., Kita, K., Miyazaki, Y., Kondo, Y., Hu, M., Shao, M., Zeng, L. M., Zhang, Y. H., Andreae, M. O., and Pöschl, U.: Aerosol optical properties in a rural environment near the mega-city Guangzhou, China: implications for regional air pollution, radiative forcing and remote sensing, Atmos. Chem. Phys., 8, 5161–5186, 2008, http://www.atmos-chem-phys.net/8/5161/2008/.
Garland, R. M., Schmid, O., Nowak, A., Achtert, P., Wiedensohler, A., Gunthe, S. S., Takegawa, N., Kita, K., Kondo, Y., Hu, M., Shao, M., Zeng, L. M., Zhu, T., Andreae, M. O., and Pöschl, U.: Aerosol optical properties observed during Campaign of Air Quality Research in Beijing 2006 (CAREBeijing-2006): Characteristic differences between the inflow and outflow of Beijing city air, J. Geophys. Res.-Atmos., 114, D00G04, doi:10.1029/2008jd010780, 2009.
Graham, B., Guyon, P., Maenhaut, W., Taylor, P. E., Ebert, M., Matthias-Maser, S., Mayol-Bracero, O. L., and Godoi, R. H. M.: Composition and diurnal variability of the natural Amazonian aerosol, J. Geophys. Res., 108, 4765, doi:10.1029/2003JD004049, 2003.

Gregory, P. H.: Distribution of Airborne Pollen and Spores and their Long-Distance Transport, Pure Appl. Geophys., 116, 309–315, 1978.
Gruber, S., Matthias-Maser, S., and Jaenicke, R.: Concentration and Chemical Composition of Aerosol Particles in Marine and Continental Air, J. Aerosol Sci., 30, S9–S10, 1999.
Hairston, P. P., Ho, J., and Quant, F. R.: Design of an instrument for real-time detection of bioaerosols using simultaneous measurement of particle aerodynamic size and intrinsic fluorescence, J. Aerosol Sci., 28, 471–482, 1997.
Hamilton, W. D. and Lenton, T. M.: Spora and Gaia: How microbes fly with their clouds, Ethol. Ecol. Evol., 10, 1–16, 1998.
Heald, C. L. and Spracklen, D. V.: Atmospheric budget of primary biological aerosol particles from fungal spores, Geophys. Res. Lett., 36, L09806, doi:10.1029/2009gl037493, 2009.
Ho, J.: Future of biological aerosol detection, Anal. Chim. Acta, 457, 125–148, 2002.
Ho, J. and Duncan, S.: Estimating aerosol hazards from an anthrax letter, J. Aerosol Sci., 36, 701–719, doi:10.1016/j.jaerosci.2004.11.019, 2005.
Huber, R., Buchner, M., Li, H. G., Schlieter, M., Speerfeld, A. D., and Riepe, M. W.: Protein binding of NADH on chemical preconditioning, J. Neurochem., 75, 329–335, 2000.
Jaenicke, R.: Abundance of cellular material and proteins in the atmosphere, Science, 308, 73–73, doi:10.1126/science.1106335, 2005.
Jaenicke, R., Matthias-Maser, S., and Gruber, S.: Omnipresence of biological material in the atmosphere, Environ. Chem., 4, 217–220, doi:10.1071/en07021, 2007.
Jones, A. M. and Harrison, R. M.: The effects of meteorological factors on atmospheric bioaerosol concentrations – a review, Sci. Total Environ., 326, 151–180, doi:10.1016/j.scitotenv.2003.11.021, 2004.
Kanaani, H., Hargreaves, M., Ristovski, Z., and Morawska, L.: Performance assessment of UVAPS: Influence of fungal spore age and air exposure, J. Aerosol Sci., 38, 83–96, doi:10.1016/j.jaerosci.2006.10.003, 2007.
Kanaani, H., Hargreaves, M., Ristovski, Z., and Morawska, L.: Deposition rates of fungal spores in indoor environments, factors effecting them and comparison with non-biological aerosols, Atmos. Environ., 42, 7141–7154, doi:10.1016/j.atmosenv.2008.05.059, 2008a.
Kanaani, H., Hargreaves, M., Smith, J., Ristovski, Z., Agranovski, V., and Morawska, L.: Performance of UVAPS with respect to detection of airborne fungi, J. Aerosol Sci., 39, 175–189, doi:10.1016/j.jaerosci.2007.10.007, 2008b.
Kaye, P. H., Stanley, W. R., Hirst, E., Foot, E. V., Baxter, K. L., and Barrington, S. J.: Single

particle multichannel bio-aerosol fluorescence sensor, Opt. Express, 13, 3583–3593, 2005.
Kell, D. B., Ryder, H. M., Kaprelyants, A. S., and Westerhoff, H. V.: Quantifying Heterogeneity – Flow Cytometry of Bacterial Cultures, Anton. Leeuw. Int. J. G., 60, 145–158, 1991.
Kenny, C. M. and Jennings, S. G.: Background bioaerosol measurements at Mace Head, J. Aerosol Sci., 29, S779–S780, doi:10.1016/S0021-8502(98)90572-9, 1998.
Kim, K. Y., Ko, H. J., Kim, H. T., Kim, Y. S., Roh, Y. M., Lee, C. M., and Kim, C. N.: Monitoring of aerial pollutants emitted from swine houses in Korea, Environ. Monit. Assess., 133, 255–266, doi:10.1007/s10661-006-9578-x, 2007.
Lacey, J. and Dutkiewicz, J.: Bioaerosols and Occupational Lung Disease, J. Aerosol Sci., 25, 1371–1404, 1994.
Lavoie, J., Dunkerley, C. J., Kosatsky, T., and Dufresne, A.: Exposure to aerosolized bacteria and fungi among collectors of commercial, mixed residential, recyclable and compostable waste, Sci. Total Environ., 370, 23–28, doi:10.1016/j.scitotenv.2006.05.016, 2006.
Law, A. K. Y., Chau, C. K., and Chan, G. Y. S.: Characteristics of bioaerosol profile in office buildings in Hong Kong, Build. Environ., 36, 527–541, 2001.
Li, J. K., Asali, E. C., and Humphrey, A. E.: Monitoring Cell Concentration and Activity by Multiple Excitation Flourometry, Biotechnol. Prog., 7, 21–27, 1991.
Linskens, H. F. and Cresti, M.: Pollen-allergy as an ecological phenomenon: a review, Plant Biosyst., 134, 341–352, 2000.
Lohmann, U. and Feichter, J.: Global indirect aerosol effects: a review, Atmos. Chem. Phys., 5, 715–737, 2005, http://www.atmos-chem-phys.net/5/715/2005/.
Martin, S. T., Andreae, M. O., Artaxo, P., Baumgartner, D., Chen, Q., Goldstein, A. H., Guenther, A., Heald, C. L., Mayol-Bracero, O. L., McMurry, P. H., Pauliquevis, T., Pöschl, U., Prather, K. A., Roberts, G. C., Saleska, S. R., Dias, M. A. S., Spracklen, D. V., Swietlicki, E., and Trebs, I.: Sources and Properties of Amazonian Aerosol Particles, Rev. Geophys., in review, 2009.
Matthias-Maser, S. and Jaenicke, R.: The size distribution of primary biological aerosol particles with radii >0.2 µm in an urban rural influenced region, Atmos. Res., 39, 279–286, 1995.
McFiggans, G., Artaxo, P., Baltensperger, U., Coe, H., Facchini, M. C., Feingold, G., Fuzzi, S., Gysel, M., Laaksonen, A., Lohmann, U., Mentel, T. F., Murphy, D. M., O'Dowd, C. D., Snider, J. R., and Weingartner, E.: The effect of physical and chemical aerosol properties on warm cloud droplet activation, Atmos. Chem. Phys., 6, 2593–2649, 2006, http://www.atmos-chem-phys.net/6/2593/2006/.
Mortazavi, R., Hayes, C. T., and Ariya, P. A.: Ice nucleation activity of bacteria isolated

from snow compared with organic and inorganic substrates, Environ. Chem., 5, 373–381, doi:10.1071/en08055, 2008.
Moschandreas, D. J., Cha, D. K., and Qian, J.: Measurement of indoor bioaerosol levels by a direct counting method, J. Environ. Eng.-ASCE, 122, 374–378, 1996.
Nikaeen, M., Hatamzadeh, M., Hasanzadeh, A., Sahami, E., and Joodan, I.: Bioaerosol emissions arising during application of municipal solid-waste compost, Aerobiologia, 25, 1–6, doi:10.1007/s10453-008-9102-6, 2009.
Pöschl, U.: Atmospheric aerosols: Composition, transformation, climate and health effects, Angew. Chem. Int. Edit., 44, 7520–7540, doi:10.1002/anie.200501122, 2005.
Pratt, K. A., DeMott, P. J., French, J. R., Wang, Z., Westphal, D. L., Heymsfield, A. J., Twohy, C. H., Prenni, A. J., and Prather, K. A.: In situ detection of biological particles in cloud ice-crystals, Nature Geosci., 2, 397–400, doi:10.1038/ngeo521, 2009.
Prenni, A. J., Petters, M. D., Kreidenweis, S. M., Heald, C. L., Martin, S. T., Artaxo, P., Garland, R. M., Wollny, A. G., and Pöschl, U.: Relative roles of biogenic emissions and Saharan dust as ice nuclei in the Amazon basin, Nature Geosci., 2, 401–404, doi:10.1038/ngeo517, 2009.
Rosenfeld, D., Lohmann, U., Raga, G. B., O'Dowd, C. D., Kulmala, M., Fuzzi, S., Reissell, A., and Andreae, M. O.: Flood or drought: How do aerosols affect precipitation?, Science, 321, 1309–1313, doi:10.1126/science.1160606, 2008.
Schnell, R. C. and Vali, G.: Atmospheric Ice Nuclei from Decomposing Vegetation, Nature, 236, 163–165, 1972.
Seedorf, J.: An emission inventory of livestock-related bioaerosols for Lower Saxony, Germany, Atmos. Environ., 38, 6565–6581, doi:10.1016/j.atmosenv.2004.08.023, 2004.
Simoneit, B. R. T. and Mazurek, M. A.: Organic Matter of the Troposphere-II. Natural Background of Biogenic Lipid Matter in Aerosols Over the Rural Western United States, Atmos. Environ., 16, 2139–2159, 1982.
Sun, J. M. and Ariya, P. A.: Atmospheric organic and bio-aerosols as cloud condensation nuclei (CCN): A review, Atmos. Environ., 40, 795–820, doi:10.1016/j.atmosenv.2005.05.052, 2006.
Wiedinmyer, C., Bowers, R. M., Fierer, N., Horanyi, E., Hannigan, M., Hallar, A. G., McCubbin, I., and Baustian, K.: The contribution of biological particles to observed particulate organic carbon at a remote high altitude site, Atmos. Environ., 43, 4278–4282, doi:10.1016/j.atmosenv.2009.06.012, 2009.

ACPD
9, 17705–17751, 2009

Table 1. Integrated number concentrations (a) and mass concentrations (b) of coarse TAP and FBAP (1–20 µm): arithmetic mean and median for each month (August–November) and for the entire measurement period (3 August–4 December 2006).

Number		Aug	Sep	Oct	Nov	Campaign
$N_{T,c}$ (cm^{-3})	Mean	0.65	0.54	1.13	1.64	1.05
	Median	0.58	0.44	0.77	1.43	0.67
$N_{F,c}$ (cm^{-3})	Mean	0.030	0.018	0.032	0.026	0.027
	Median	0.025	0.014	0.024	0.018	0.020
$N_{F,c}/N_{T,c}$ (%)	Mean	5.36	3.89	4.12	2.61	3.90
	Median	4.81	3.60	3.43	1.81	3.30
Mass		**Aug**	**Sep**	**Oct**	**Nov**	**Campaign**
$M_{T,c}$ (µg m^{-3})	Mean	5.32	6.07	8.63	8.17	7.30
	Median	4.56	4.83	6.36	7.33	5.62
$M_{F,c}$ (µg m^{-3})	Mean	1.03	1.09	1.94	0.92	1.26
	Median	0.80	0.80	1.40	0.64	0.86
$M_{F,c}/M_{T,c}$ (%)	Mean	20.9	19.3	24.5	14.4	19.5
	Median	19.9	18.8	23.2	12.1	18.5

ACPD
9, 17705–17751, 2009

Table A1. List of frequently used acronyms and symbols.

Acronym/Symbol	Unit	Description
PBAP		primary biological aerosol particle
FBAP		fluorescent biological aerosol particle
FAP		fluorescent aerosol particle
NAP		non-fluorescent aerosol particle
TAP		total aerosol particle (including fluorescent and non-fluorescent)
N	cm^{-3}	particle number concentration
N_F	cm^{-3}	N of fluorescent particles (fluorescence bins >3)
$N_{F,c}$	cm^{-3}	N of coarse fluorescent particles ($D_{a,g}$ 1.037–19.81 µm, size bins 10–51); taken as the number concentration of coarse FBAPs
N_T	cm^{-3}	N of all particles (TAPs, including fluorescent and non-fluorescent)
$N_{T,c}$	cm^{-3}	N of all coarse particles (coarse TAPs, including fluorescent and non-fluorescent)
M	$\mu g\,m^{-3}$	particle mass concentration
M_F	$\mu g\,m^{-3}$	M of fluorescent particles
$M_{F,c}$	$\mu g\,m^{-3}$	M of coarse fluorescent particles ($D_{a,g}$ 1.037–19.81 µm, size bins 10–51); taken as the mass concentration of coarse FBAPs
M_T	$\mu g\,m^{-3}$	M of all particles (TAPs, including fluorescent and non-fluorescent)
$M_{T,c}$	$\mu g\,m^{-3}$	M of all coarse particles (coarse TAPs, including fluorescent and) non-fluorescent)
D_a	µm	aerodynamic particle diameter
$D_{a,g}$	µm	geometric mean aerodynamic particle diameter (size bin or lognormal fit)
σ_g	–	geometric standard deviation of lognormal fit)

ACPD
9, 17705–17751, 2009

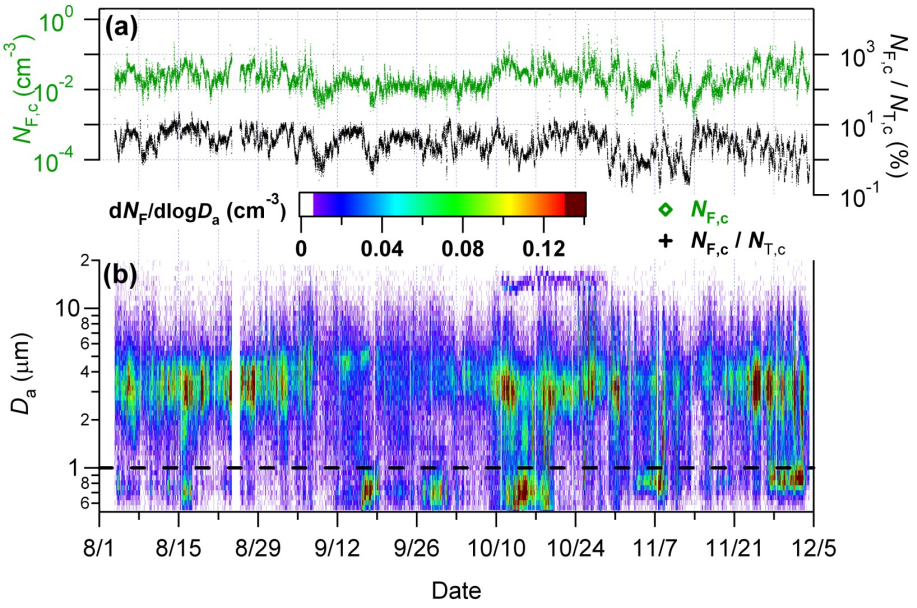

Fig. 1. Time series of FBAP number concentrations and size distributions for the entire measurement period (3 August–4 December 2006). **(a)** Integrated coarse FBAP concentration (1–20 µm, $N_{F,c}$) on left axis (green) and FBAP fraction of TAP number ($N_{F,c}/N_{T,c}$) on right axis (black). Note that axes are logarithmically scaled and off-set from one another. Each data point represents a 5 min measurement. **(b)** FBAP size distribution with date on x-axis, aerodynamic diameter on y-axis, and color scale of dN_F/dlogD_a with white values set to $LDC_{dN/dlogD_a}=6.4\times10^{-3}$ cm^{-3}. Dashed black line at 1.0 µm shows particle size cut-off below which fluorescent particles were not considered FBAP due to interference with non-biological aerosol.

ACPD
9, 17705–17751, 2009

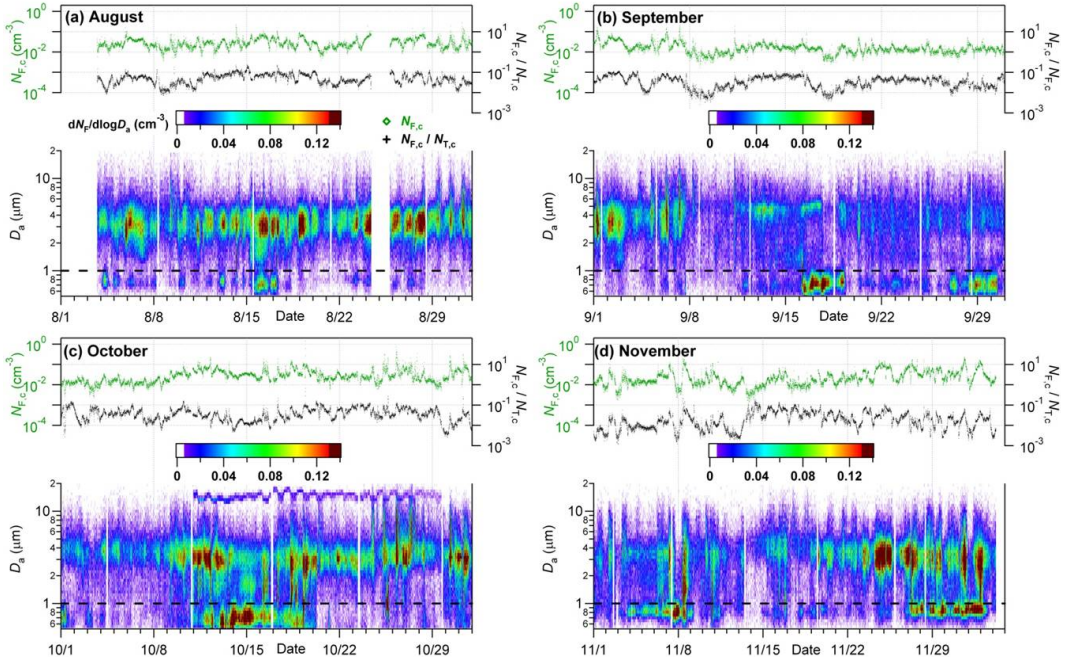

Fig. 2. Time series of FBAP number concentrations (panel top halves) and size distributions (panel bottom halves) for each month of the measurement period (plots analogous to Fig. 1): **(a)** August, **(b)** September, **(c)** October, and **(d)** November (extending to 4 December).

ACPD
9, 17705–17751, 2009

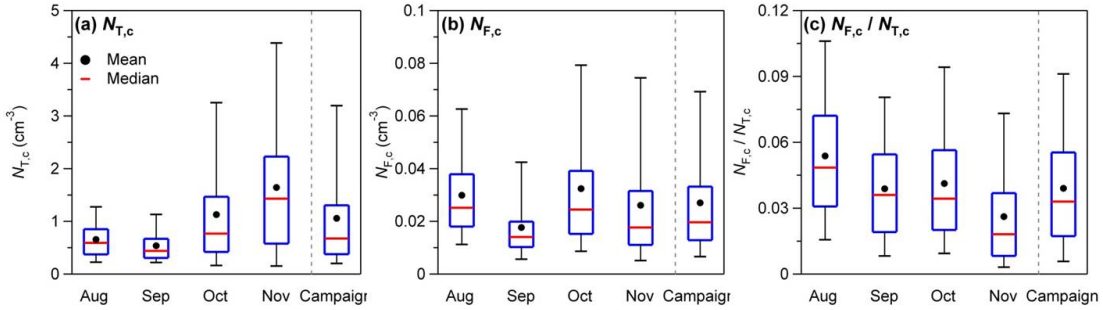

Fig. 3. Statistical distribution of integrated coarse TAP and FBAP number concentrations (1–20 µm) measured during each month (August–November) and over the full campaign as box-whisker plots. Black dot represents arithmetic mean, red bar represents median (50th percentile), lower and upper limits of blue box represent 25th and 75th percentiles, respectively, and horizontal bars at the end of lower and upper vertical bars represent 5th and 95th percentiles, respectively. **(a)** $N_{T,c}$, **(b)** $N_{F,c}$, **(c)** $N_{F,c}/N_{T,c}$.

ACPD
9, 17705–17751, 2009

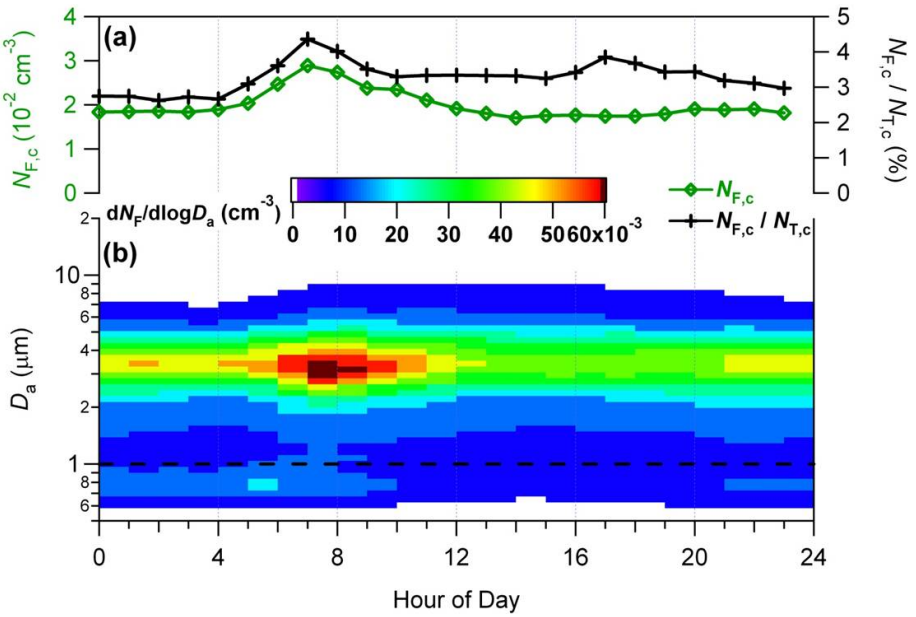

Fig. 4. Diel cycles of FBAP number concentrations and size distributions for the entire measurement period (hourly median values vs. local time of day). **(a)** Integrated coarse FBAP concentration (1–20 µm, $N_{F,c}$) on left axis (green) and FBAP fraction of TAP number ($N_{F,c}/N_{T,c}$) on right axis (black). **(b)** FBAP size distribution with hour of day on x-axis, aerodynamic diameter on y-axis and color scale of $dN_F/d\log D_a$ with white values set to 0.001 cm^{-3} for visual clarity. Dashed black line at 1.0 µm shows particle size cut-off below which fluorescent particles were not considered FBAP due to interference with non-biological aerosol.

ACPD
9, 17705–17751, 2009

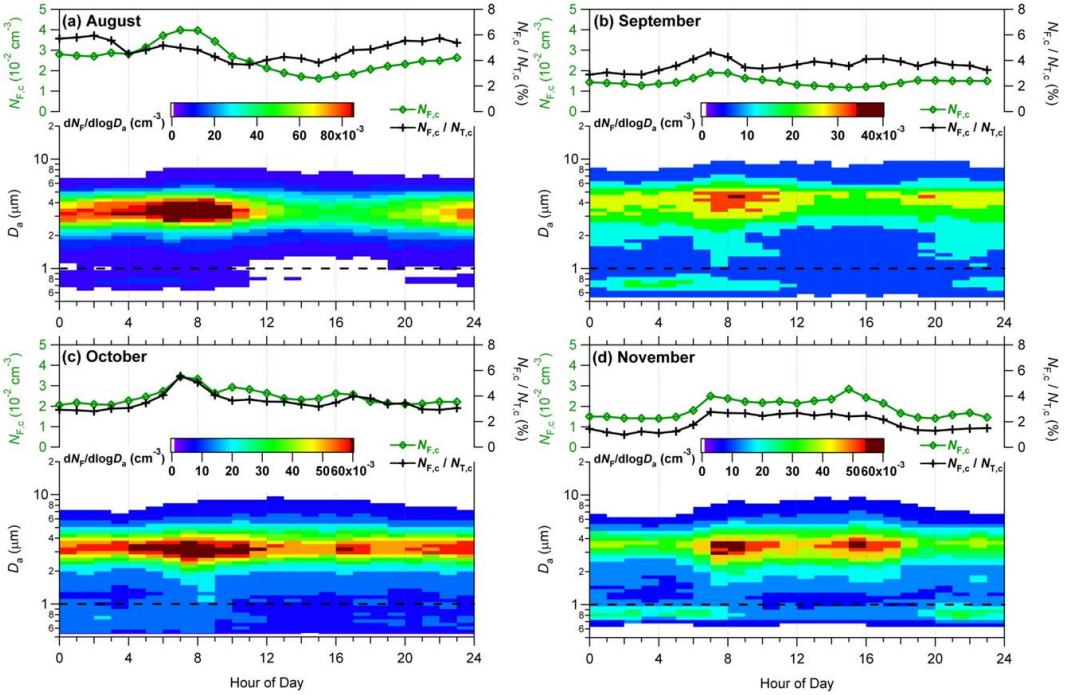

Fig. 5. Diel cycles of FBAP number concentrations (panel top halves) and size distributions (panel bottom halves) for each month of the measurement period (plots analogous to Fig. 4): **(a)** August, **(b)** September, **(c)** October, and **(d)** November.

ACPD
9, 17705–17751, 2009

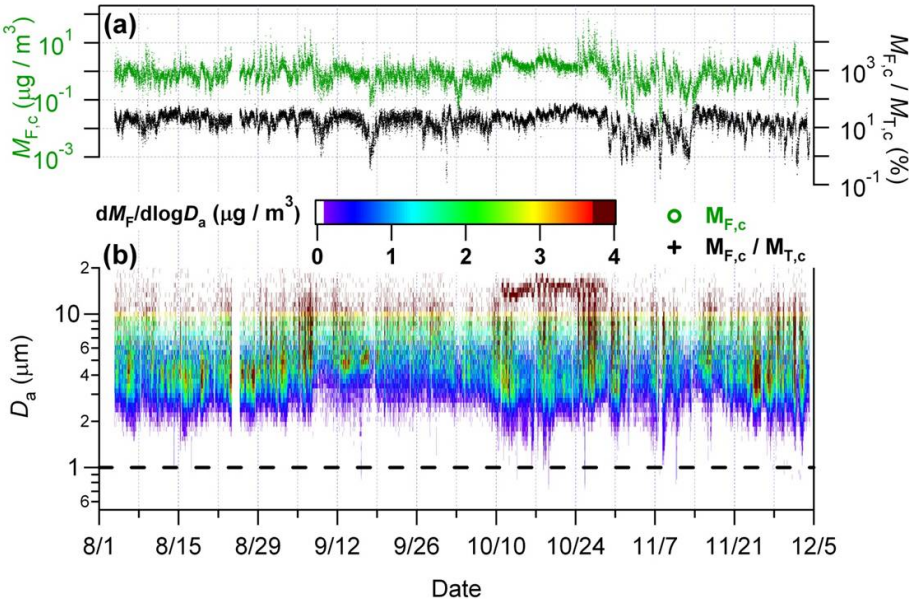

Fig. 6. Time series of FBAP mass concentrations and size distributions for the entire measurement period. **(a)** Integrated coarse FBAP mass concentration (1–20 µm, $M_{F,c}$) on left axis (green) and FBAP fraction of TAP mass ($M_{F,c}/M_{T,c}$) on right axis (black). Note that axes are logarithmically scaled and off-set from one another. Each data point represents a 5 min measurement. **(b)** FBAP size distribution with date on x-axis, aerodynamic diameter on y-axis, and color scale of dM_F/dlogD_a with white values set to 0.1 µg/m^3 for visual clarity. Dashed black line at 1.0 µm shows particle size cut-off below which fluorescent particles were not considered FBAP due to interference with non-biological aerosol.

ACPD
9, 17705–17751, 2009

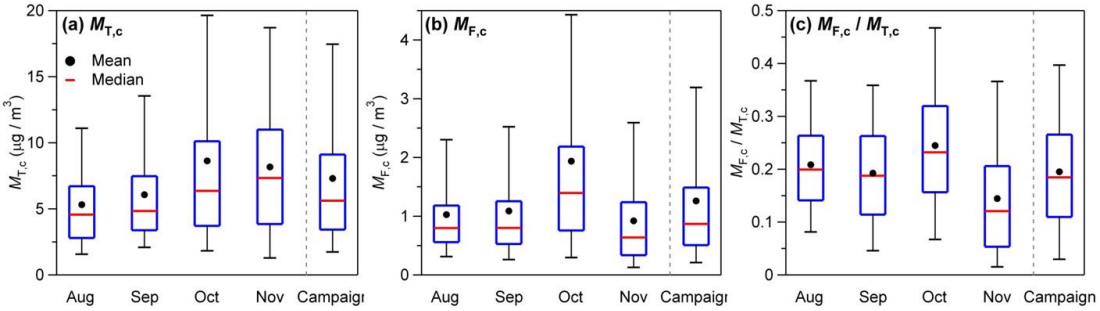

Fig. 7. Statistical distribution of integrated coarse TAP and FBAP mass concentrations (1–20 µm) measured during each month (August–November) and over the full campaign as box-whisker plots (plots analogous to Fig. 3): **(a)** $M_{T,c}$, **(b)** $M_{F,c}$, **(c)** $M_{F,c}/M_{T,c}$.

ACPD
9, 17705–17751, 2009

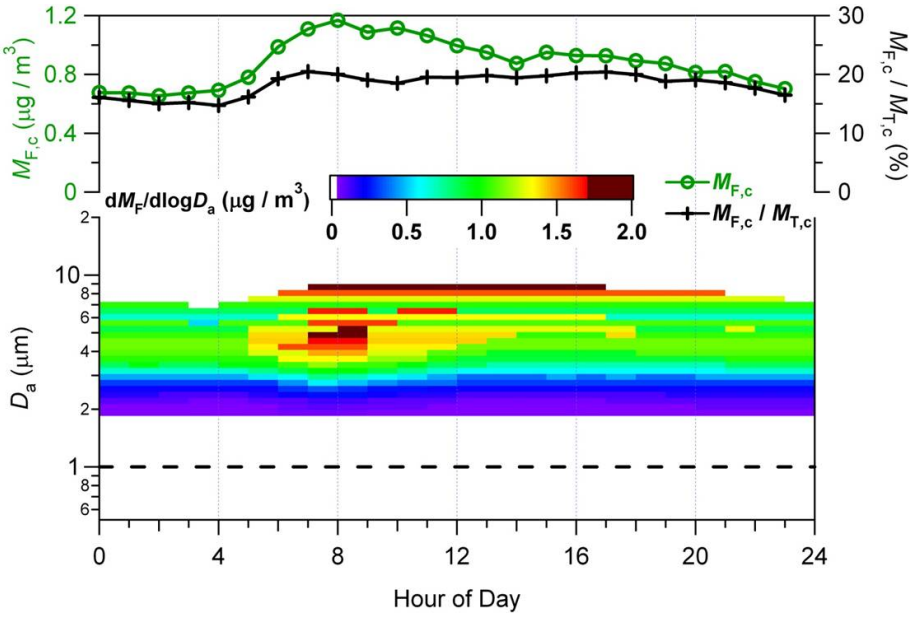

Fig. 8. Diel cycles of FBAP mass concentrations and size distributions for the entire measurement period (hourly median values vs. local time of day). (a) Integrated coarse FBAP concentration (1–20 µm, $M_{F,c}$) on left axis (green) and FBAP fraction of TAP mass ($M_{F,c}/M_{T,c}$) on right axis (black). (b) FBAP mass size distribution with hour of day on x-axis, aerodynamic diameter on y-axis, and color scale of dM_F/dlogD_a with white values set to 0.04 µg/m^3 for visual clarity. Dashed black line at 1.0 µm shows particle size cut-off below which particles were not considered FBAP due to interference with non-biological aerosol. Sharp cut-off in mass concentration above 10.5 µm is due to counting statistics and use of median values in this plot (i.e., above this size more than 50% of 5 L sample volumes contained no FBAP).

ACPD
9, 17705–17751, 2009

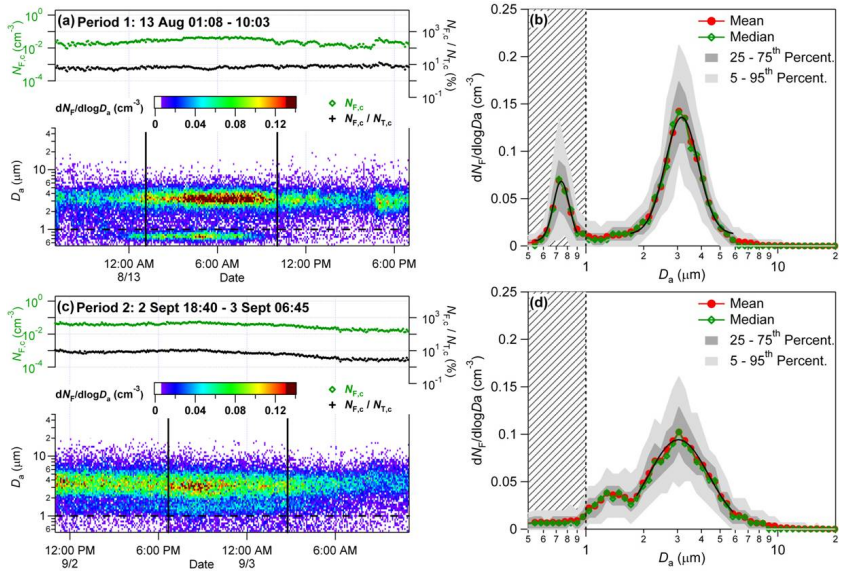

Fig. 9. Characteristic FBAP number size distribution patterns observed during exemplary periods #1 and #2. Left panels show time series of $N_{F,c}$, $N_{F,c}/N_{T,c}$ ratio and $dN_F/d\log D_a$ on days of interest (analogous to Fig. 1), and black vertical lines indicate time periods over which exemplary size distributions were averaged ($dN_F/d\log D_a$ vs. D_a, right panels). Red traces represent mean values, green traces represent median values, dark gray regions show 25–75th percentile range, and light gray regions show 5–95th percentile range. Hatched area below 1.0 µm indicates particle size range where fluorescent particles were not considered FBAP due to interference with non-biological aerosol. Black traces are lognormal fits to individual peaks (mean values) with the following fit parameters: **(a, b)** Period #1; Fit 1.1: D_a=0.54–0.90 µm, $D_{a,g}$=0.74 µm, σ_g=1.10, N=6.5×10^{-3} cm^{-3}; Fit 1.2: D_a=1.7–5.8 µm; $D_{a,g}$=3.2 µm, σ_g=1.22, N=2.7×10^{-2} cm^{-3}; **(c, d)** Period #2; Fit 2.1: D_a=1.8–5.8 µm; $D_{a,g}$=3.0 µm, σ_g=1.43, N=3.7×10^{-2} cm^{-3}.

ACPD
9, 17705–17751, 2009

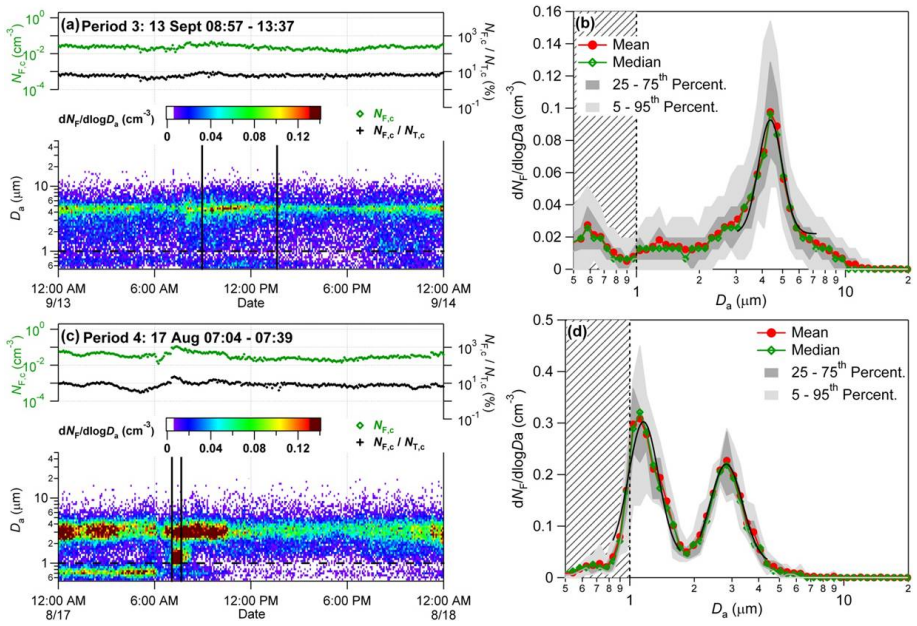

Fig. 10. Characteristic FBAP number size distribution patterns observed during exemplary periods #3 and #4 (plots analogous to Fig. 9). **(a, b)** Period #3; Fit3.1: D_a=3.0–7.2 µm; $D_{a,g}$ = 4.4 µm, σ_g=1.14, N=1.0×10^{-2} cm^{-3}; **(c, d)** Period #4; Fit 4.1: D_a=0.84–1.7 µm; $D_{a,g}$=1.2 µm, σ_g=1.18, N=4.0×10^{-2} cm^{-3}; Fit 4.2: D_a=2.1–4.4 µm; $D_{a,g}$=2.8 µm, σ_g=1.19, N=2.8×10^{-2} cm^{-3}.

ACPD
9, 17705–17751, 2009

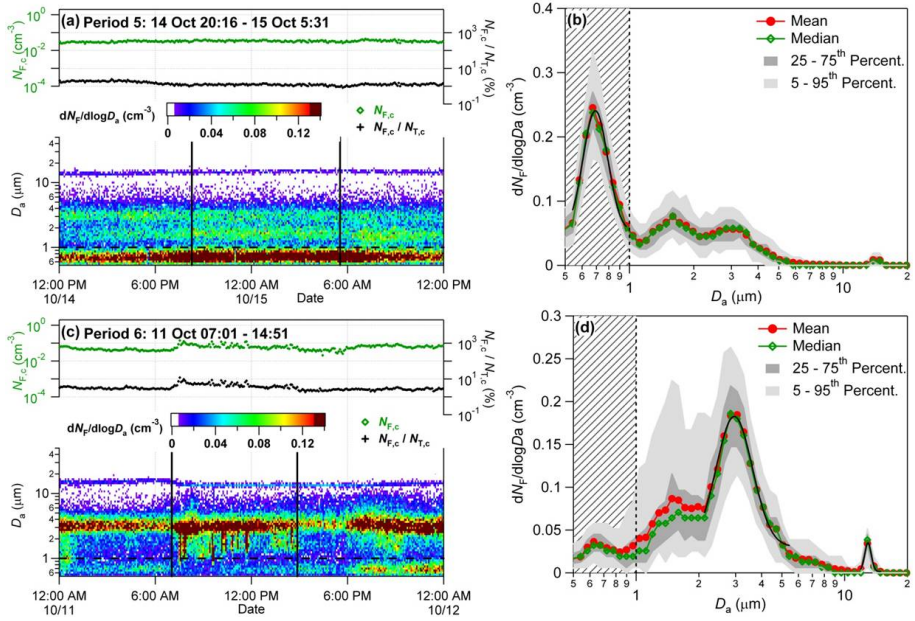

Fig. 11. Characteristic FBAP number size distribution patterns observed during exemplary periods #5 and #6 (plots analogous to Fig. 9). **(a, b)** Period #5; Fit5.1: D_a=0.54–0.96 µm; $D_{a,g}$=0.74 µm, σ_g=1.14, N=2.7×10^{-1} cm^{-3}; **(c, d)** Period #6; Fit 6.1: D_a=2.1–5.4 µm; $D_{a,g}$=3.0 µm, σ_g=1.22, N =3.3×10^{-2} cm^{-3}; Fit 6.2: D_a=12.0–14.9 µm; $D_{a,g}$=13.0 µm, σ_g=1.04, N=1.30×10^{-3} cm^{-3}.

ACPD
9, 17705–17751, 2009

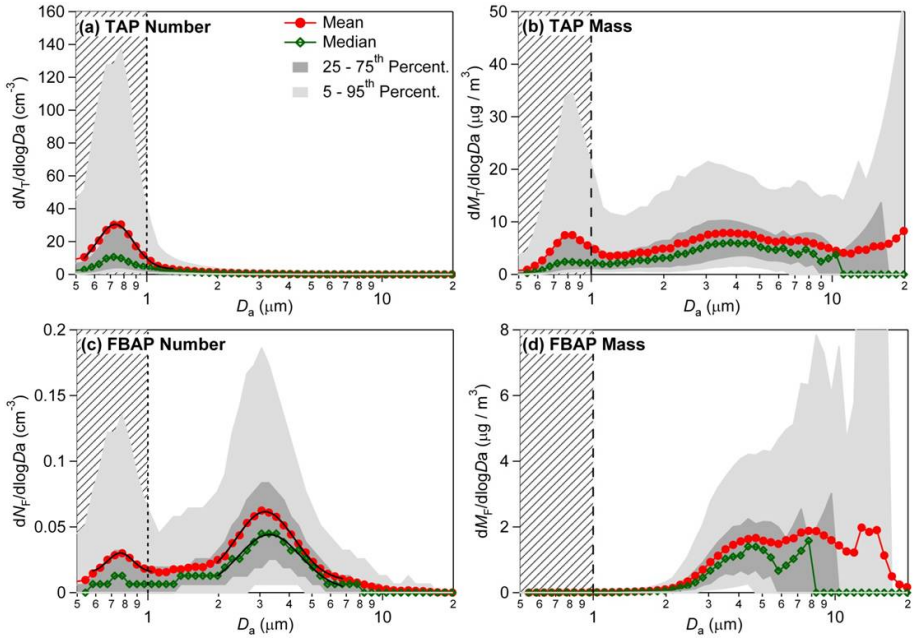

Fig. 12. Average particle number and mass size distributions for the entire measurement period. Red traces represent mean values, green traces represent median values, dark gray regions show 25–75th percentile range, and light gray regions show 5–95th percentile range. Hatched area below 1.0 μm indicates particle size range where fluorescent particles were not considered FBAP due to interference with non-biological aerosol. Black traces are lognormal fits to individual peaks with the following fit parameters: **(a)** TAP number ($dN_T/dlogD_a$): Fit N_T: D_a=0.54–1.3 μm; $D_{a,g}$=0.74 μm, σ_g=1.20, N=5.3 cm^{-3}, **(b)** TAP Mass ($dM_T/dlogD_a$); **(c)** FBAP Number ($dN_F/dlogD_a$); Fit N_F-1 (mean): D_a=0.58–1.0 μm; $D_{a,g}$=0.76 μm, σ_g=1.13, N =2.0×10^{-3} cm^{-3}; Fit N_F-2 (mean): D_a=2.0–6.7 μm; $D_{a,g}$=3.2 μm, σ_g=1.33, N=1.6×10^{-2} cm^{-3}, Fit N_F-3 (median): D_a= 2.0–6.7 μm; $D_{a,g}$=3.3 μm, σ_g=1.36, N=1.4×10^{-2}cm^{-3}; **(d)** FBAP Mass: $dM_F/dlogD_a$.

ACPD
9, 17705–17751, 2009

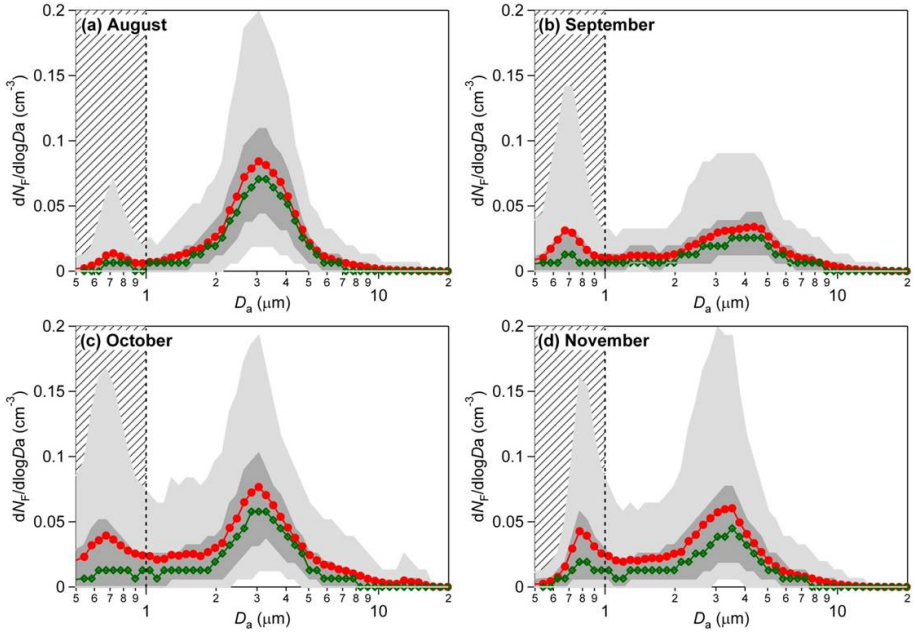

Fig. 13. Average FBAP number size distributions for each month of the measurement period (plots analogous to Fig. 12): **(a)** August, **(b)** September, **(c)** October, **(d)** November.

ACPD
9, 17705–17751, 2009

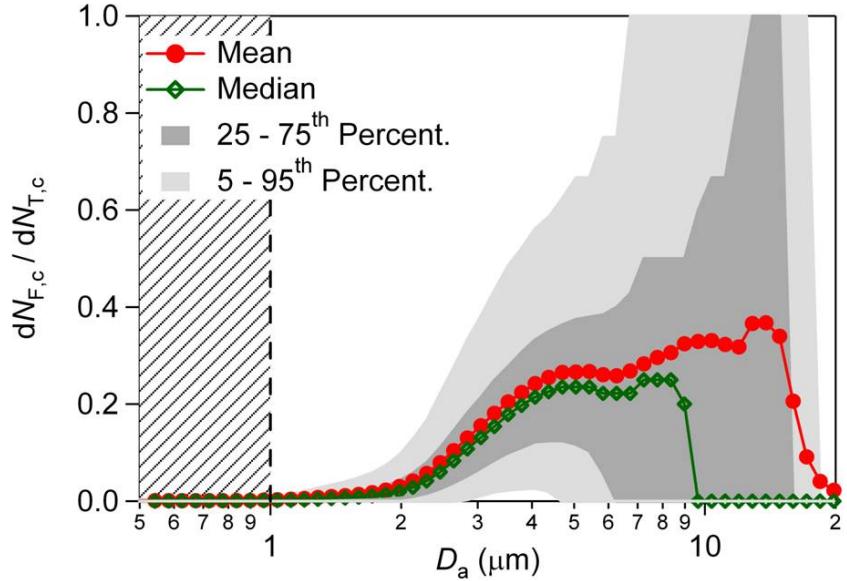

Fig. 14. Average size distribution of the FBAP to TAP number concentration ratio ($dN_{F,c}/dN_{T,c}$) for the entire measurement period (plot analogous to Fig. 12).

ACPD

9, 17705–17751, 2009